

EVOLUTION IN THE HALO MASSES OF ISOLATED GALAXIES BETWEEN $z \sim 1$ AND $z \sim 0$: FROM DEEP2 TO SDSS

CHARLIE CONROY¹, FRANCISCO PRADA¹, JEFFREY A. NEWMAN², DARREN CROTON³, ALISON L. COIL⁴, CHRISTOPHER J. CONSELICE⁵, MICHAEL C. COOPER³, MARC DAVIS^{3,6}, S. M. FABER⁷, BRIAN F. GERKE⁶, PURAGRA GUHATHAKURTA⁷, ANATOLY KLYPIN⁸, DAVID C. KOO⁷, RENBIN YAN³

Draft version July 1, 2018

ABSTRACT

We measure the evolution in the virial mass-to-light ratio (M_{200}/L_B) and virial-to-stellar mass ratio (M_{200}/M_*) for isolated $\sim L^*$ galaxies between $z \sim 1$ and $z \sim 0$ by combining data from the DEEP2 Galaxy Redshift Survey and the Sloan Digital Sky Survey. Utilizing the motions of satellite galaxies around isolated galaxies, we measure line-of-sight velocity dispersions and derive dark matter halo virial masses for these host galaxies. At both epochs the velocity dispersion of satellites correlates with host galaxy stellar mass, $\sigma \propto M_*^{0.4 \pm 0.1}$, while the relation between satellite velocity dispersion and host galaxy B -band luminosity may grow somewhat shallower from $\sigma \propto L_B^{0.6 \pm 0.1}$ at $z \sim 1$ to $\sigma \propto L_B^{0.4 \pm 0.1}$ at $z \sim 0$. The evolution in M_{200}/M_* from $z \sim 1$ to $z \sim 0$ displays a bimodality insofar as host galaxies with stellar mass below $M_* \sim 10^{11} h^{-1} M_\odot$ maintain a constant ratio (the intrinsic increase is constrained to a factor of 1.1 ± 0.7) while host galaxies above $M_* \sim 10^{11} h^{-1} M_\odot$ experience a factor of 4 ± 3 increase in their virial-to-stellar mass ratio. This result can be easily understood if galaxies below this stellar mass scale continue to form stars while star formation in galaxies above this scale is quenched and the dark matter halos of galaxies both above and below this scale grow in accordance with Λ CDM cosmological simulations. Host galaxies that are red in $U - B$ color have larger satellite dispersions and hence reside on average in more massive halos than blue galaxies at both $z \sim 1$ and $z \sim 0$. The satellite population of host galaxies varies little between these epochs; the only significant difference is that satellites at $z \sim 1$ tend to be comparatively fainter (by ~ 0.15 magnitudes in the mean) relative to their host luminosity than satellites at $z \sim 0$. The redshift and host galaxy stellar mass dependence of M_{200}/M_* agrees qualitatively with the Millennium Run semi-analytic model of galaxy formation.

Subject headings: galaxies: evolution — galaxies: kinematics and dynamics — galaxies: halos

1. INTRODUCTION

The current cosmological framework indicates that galaxies are embedded in massive dark matter halos that extend far beyond the visible baryonic component. The virial mass-to-light, M_{200}/L , and virial-to-stellar mass, M_{200}/M_* , ratios provide simple distillations of the complex interplay between galaxies and their dark matter halos. Constraints on the dependence of M_{200}/L and M_{200}/M_* on galaxy properties and redshift hence afford unique insight into the formation and evolution of galaxies in a cosmological context. For example, evolution of M_{200}/M_* provides constraints on the evolution of star formation efficiency in galaxies.

Yet there are surprisingly few direct constraints on

M_{200}/L or M_{200}/M_* . Since dark matter extends far beyond the visible components of a galaxy, it is in practice difficult to probe the halo mass on large scales (i.e., $\gtrsim 100 h^{-1}$ kpc) due to a lack of luminous tracers. The halo masses of clusters of galaxies can be estimated by strong and weak gravitational lensing, the tight relationship between the X-ray temperature of the diffuse intra-cluster medium and the dark matter halo, the Sunyaev-Zeldovich effect, and by measuring the velocity dispersion of the cluster galaxies themselves, under the assumption that the cluster galaxies are tracing out the dark matter halo potential (see Voit 2005, for a recent review).

Probing the halos of isolated galaxies is more difficult. The only methods that are currently capable of directly probing the halo mass of isolated $\sim L^*$ galaxies to large radii are weak lensing (Brainerd et al. 1996; Wilson et al. 2001; Guzik & Seljak 2002; Hoekstra et al. 2004, 2005; Kleinheinrich et al. 2005; Mandelbaum et al. 2006) and satellite dynamics (Little & Tremaine 1987; Erickson et al. 1987, 1999; Zaritsky et al. 1993, 1997; McKay et al. 2002; Prada et al. 2003; Brainerd & Specian 2003; Brainerd 2005; van den Bosch et al. 2004; Conroy et al. 2005b), which utilizes satellite galaxies as test particles that trace out the dark matter halo velocity field out to several hundred kiloparsecs. One limitation of both techniques is that they must “stack” many isolated galaxies in order to build up a robust signal. Both methods have yielded

¹ Instituto de Astrofísica de Andalucía (CSIC), E-18008 Granada, Spain

² Hubble Fellow, Lawrence Berkeley National Laboratory, 1 Cyclotron Road, Berkeley, CA 94720

³ Department of Astronomy, University of California, Berkeley, CA 94720

⁴ Hubble Fellow, Steward Observatory, University of Arizona, Tucson, AZ 85721

⁵ School of Physics and Astronomy, University of Nottingham, NG7 2RD, UK

⁶ Department of Physics, University of California, Berkeley, CA 94720

⁷ University of California Observatories/Lick Observatory, Department of Astronomy and Astrophysics, University of California, Santa Cruz, CA 95064

⁸ Department of Astronomy, New Mexico State University, Box 30001, Department 4500, Las Cruces, NM 88003

similar results; e.g., each finds a positive correlation between galaxy luminosity and the virial mass of its dark matter halo.

The evolution in the virial mass-to-light ratios of bright isolated galaxies is only poorly constrained. Wilson et al. (2001) measured the weak lensing signal for early-type $\sim L^*$ galaxies from $z = 0.8$ to $z = 0.1$. They found little evolution in the halo mass of $\sim L^*$ galaxies, though their formal errors on the halo mass at $z \sim 0.8$ were $\gtrsim 50\%$. Furthermore, that work assumed that L^* did not evolve with redshift and that halo mass was proportional to the square root of galaxy luminosity. Most recently, utilizing stellar masses and weak lensing data from COMBO-17 and GEMS, Heymans et al. (2006) find no significant evolution in the virial-to-stellar mass ratios of bright galaxies to $z \sim 0.8$ (though constraints are weak; they find that the ratio decreases by no more than a factor of 2.6 at 1σ).

Using the first $\sim 25\%$ of the recently completed DEEP2 redshift survey, which has now collected spectra for $> 40,000$ galaxies at $0.7 < z < 1.4$, Conroy et al. (2005b) used the dynamics of satellite galaxies to measure the halo mass for bright isolated galaxies with satellites (referred to as “host” galaxies) and compared their derived M/L to measurements from the Sloan Digital Sky Survey (SDSS) at $z \sim 0$. However, the small sample size and differences in selection effects between DEEP2 and SDSS meant that all claims in that work had to be highly qualified.

This study presents a much more detailed comparison between host-satellite systems identified in the completed DEEP2 Redshift Survey and systems found in a consistent way from the fourth public data release of the SDSS. The increased data sample at $z \sim 1$, combined with a careful handling of the different selection effects between the two surveys, allows a robust determination of the evolution in the B -band virial mass-to-light ratio and the virial-to-stellar mass ratio of $\sim L^*$ host galaxies from $z \sim 1$ to $z \sim 0$.

The classic Tully-Fisher relation is also capable of constraining the halo mass of isolated disk-dominated galaxies, though the steps required to convert the observed rotation speed into a dark matter halo virial mass is more model dependent than either weak lensing or satellite dynamics. (van den Bosch 2002; Kassin et al. 2006b; Gnedin et al. 2006). In particular, this method must extrapolate the rotation curve far beyond the region covered by observations and/or requires knowledge of the relative contribution of baryonic and dark matter to the observed rotation curve as a function of scale (see, e.g., Gnedin et al. 2006). Recently, Conselice et al. (2005), Boehm & Ziegler (2006), and Kassin et al. (2006a) have used the Tully-Fisher relation to constrain the evolution in the virial-to-stellar mass ratio from $z \sim 1$ to $z \sim 0$. These studies found no evidence for a change in this ratio, though their sample sizes were relatively small compared to weak lensing and satellite kinematics studies (~ 100 objects for the first two studies and ~ 550 for the last).

This article proceeds in the following manner: §2 outlines our definition for host and satellite galaxies and describes our method for estimating halo masses of host galaxies. In §3 we describe the galaxy surveys studied and explain the methods used to mitigate survey selection effects. §4 contains a comparison of the properties of

host and satellite galaxies between $z \sim 1$ and $z \sim 0$, and in §5 we present satellite velocity dispersions and derived virial mass-to-light and virial-to-stellar mass ratios as a function of host galaxy redshift, luminosity, stellar mass, and color. §6 contains a comparison between our results and a semi-analytic model of galaxy evolution. In §7 we discuss these results and §8 concludes. Those readers not interested in the technical details should focus on §§ 4 – 8.

A Λ CDM cosmology is adopted throughout: $\Omega_m = 1 - \Omega_\Lambda = 0.3$, with $H_0 = 100h$ km s $^{-1}$ Mpc $^{-1}$. All absolute magnitudes quoted here are in the AB system (Oke & Gunn 1983), and throughout magnitudes are quote as $M_B - 5\log(h)$. We adopt a mass definition for dark matter halos such that the virial radius of a halo corresponds to a region with mean density 200 times the critical density, denoted r_{200} . The halo mass is the mass interior to r_{200} , and is denoted M_{200} . M_* is reserved for stellar masses and M^* for the characteristic scale of the luminosity function.

2. METHODOLOGY

This section describes our definitions of host and satellite galaxies and our methods for determining line-of-sight velocity dispersions and dark matter halo masses of host galaxies.

2.1. Isolation and Satellite Criteria

The use of satellite dynamics for extracting mass estimates of their host galaxies is motivated by a scenario in which a bright galaxy resides at rest at the center of its dark matter halo, has no other bright companions, and is surrounded by faint satellites that are bound to the host halo and orbit within it. The criteria used to define host galaxies and their associated satellites are meant to capture such systems. Note that, according to our use, “host” galaxies are not completely isolated; rather they are isolated with respect to other comparably bright galaxies. These criteria reject objects in dense regions such as clusters and groups, which typically contain several comparably bright galaxies.

Isolation criteria is specified using three parameters: an absolute B -band magnitude difference, ΔM_B , a velocity difference, ΔV , and a projected physical separation ΔR_p . The latter two parameters define a search cylinder: if a galaxy has no companions within the search cylinder that are within ΔM_B in absolute magnitude, then it is deemed to be “isolated”.

With a set of isolated galaxies we then search for satellite companions by specifying a set of three similar parameters: a magnitude difference, δM_B , a velocity difference, δV , and a projected physical separation, δR_p (here and throughout we reserve Δ for isolation criteria and δ for satellite criteria). We then search for companions of the isolated galaxies that are within the search cylinder defined by δV and δR_p , and are fainter than the isolated galaxy by at least δM_B magnitudes. Isolated galaxies with satellites are called “host galaxies”.

Various authors have used different parameters for identifying host-satellite systems and have found that the resulting derived halo mass is quite insensitive to reasonable choices of parameters (Prada et al. 2003; Conroy et al. 2005b). In this work we use the search parameters listed in Table 1; the same parameters are

TABLE 1
SEARCH CRITERIA

Sample Name	Isolation Criteria			Satellite Criteria		
	ΔM_B	ΔV km s ⁻¹	ΔR_p h ⁻¹ kpc	δM_B	δV km s ⁻¹	δR_p h ⁻¹ kpc
A	1.0	1000	500	1.0	750	350
B	1.5	1000	500	1.5	750	350
C	1.5	1000	1000	1.5	500	350

NOTE. — The ΔV and δV parameters are set to larger values when considering samples of brighter host galaxies. See §2.1 for details.

used to extract systems from both the DEEP2 and SDSS surveys, and our fiducial set of parameters is sample *A*. In Appendix B we show that our results are unchanged within 1σ when adopting different search parameters.

However, the recovered satellite velocity dispersion (see below) can become sensitive to δV (the maximum velocity separation between host and satellite) when the contribution from the true satellite dispersion is significant even at the edge of the dV distribution (the window defined by $\pm\delta V$). This problem is alleviated simply by increasing the δV parameter for brighter host galaxies (which have larger satellite dispersions). Indeed, tests with simulations have shown that scaling the δV parameter with host galaxy luminosity more robustly recovers the true satellite dispersion at large host luminosities (van den Bosch et al. 2004; Chen et al. 2005). Hence for the highest host galaxy luminosity and stellar mass bins at $z \sim 0$ and $z \sim 1$, we increase δV by increments of 500 km s⁻¹ until the measured dispersion has converged (the satellite dispersion for fainter samples had already converged using sample *A* parameters). Convergence is achieved when using $\delta V = 1000$ km s⁻¹ for all of these bins except for the highest stellar mass bin at $z \sim 0$; there the dispersion converges at $\delta V = 1500$ km s⁻¹.⁹

2.2. Velocity Dispersion & Halo Mass Estimation

This section describes in detail how to estimate the dark matter halo mass of host galaxies. This procedure can be conceptually separated into three steps: identifying host-satellite systems in a galaxy catalog; reconstructing the line-of-sight velocity dispersion profile of their satellites; and converting the dispersion profile into a mass. Once host-satellite systems are found, the velocity dispersion profile¹⁰ of the host galaxy dark matter halo can be estimated from the distribution of velocity differences between host and satellite galaxies, $dV \equiv V_{\text{host}} - V_{\text{sat}}$, in bins of projected distance from the host galaxy, R_p .

In an ideal world there would exist hundreds of sufficiently luminous satellite galaxies per host galaxy, and the task of measuring a velocity dispersion profile would be comparatively straightforward. Unfortunately, in

practice there are on average only 1 – 2 satellites per host galaxy, due to the magnitude limit of the redshift surveys used here (most isolated galaxies possess *no* identifiable satellites). In order to build up a dispersion profile we must combine satellites from many host galaxies and construct an average profile around an average host (e.g. Zaritsky & White 1994). Assuming that host galaxy properties such as luminosity are tightly correlated with their dark matter halo mass, then by stacking host galaxies in bins of luminosity we can recover the average underlying halo mass (Prada et al. 2003). Weak lensing studies rely on the same stacking procedure, since the lensing signal from individual isolated galaxies is very weak (e.g., Brainerd et al. 1996).

Naively, one might expect the velocity distribution of satellites, $f(dV)$, to be approximately Gaussian with σ given by the velocity dispersion of satellite galaxies associated with the host galaxy (Prada et al. 2003). In fact, there is a significant contribution to the dV distribution from so-called “interloper” galaxies. Interlopers are galaxies that are classified as satellites in projection but are in fact not true satellites, i.e., they are not physically associated with the host galaxy.

Previous authors (e.g., McKay et al. 2002; Prada et al. 2003; Conroy et al. 2005b) have modeled the effect of interlopers as a constant contribution to $f(dV)$ at all velocities. Tests with simulations have confirmed that modeling interlopers in this way results in a robust recovery of the underlying mass distribution (see Appendix C). However, van den Bosch et al. (2004) and Chen et al. (2005) found that in mock galaxy catalogs interlopers do not have a constant dV distribution but rather have a velocity structure somewhat similar to true satellites (though in the mock catalogs the width of the interloper distribution does not appear to scale with host galaxy luminosity). Despite this (or perhaps *because* of this), these authors found that modeling the interloper distribution as a constant component to the dV distribution does yield an accurate recovery of the velocity dispersion profile as well as the underlying halo mass, in agreement with previous work.

Hence $f(dV)$ is modeled as a Gaussian distribution plus a constant component:

$$f(dV; \eta, \sigma_{\text{los}}) = \frac{\eta}{2\delta V} + \frac{1 - \eta}{\sqrt{2\pi} \sigma \text{erf}(\delta V/\sqrt{2}\sigma)} e^{-dV^2/(2\sigma_{\text{los}}^2)}, \quad (1)$$

subject to the following normalization condition:

$$\int_{-\delta V}^{+\delta V} f(dV; \eta, \sigma_{\text{los}}) d(dV) = 1, \quad (2)$$

where η is the fraction of interlopers within $\pm\delta V$ and σ_{los} is the line-of-sight satellite dispersion.

We use a maximum-likelihood method to fit this Gaussian-plus-constant function to the observed distribution of dV for pairs in some bin of projected separation R_p . We maximize the likelihood function:

$$\ln[L(\eta, \sigma_{\text{los}})] = \sum_i \lambda_i \ln[f(dV_i; \eta, \sigma_{\text{los}})] \quad (3)$$

over a dense grid in σ_{los} and η , where dV_i is the dV value for the i th satellite–host galaxy pair, which is given weight λ_i (see below). Since we only use dV_i values for

⁹ In addition, for this case ΔV has been increased to 1500 km s⁻¹ since it is conceptually awkward for δV to be larger than ΔV .

¹⁰ Note that what is actually being probed is the *line-of-sight* velocity dispersion profile; we drop ‘line-of-sight’ in the remainder of this paper for brevity.

pairs in some bin of projected separation, the parameters η and σ_{los} are implicit functions of R_p .

In the following analysis satellite i is assigned a weight λ_i according to the inverse number of satellites associated with the host of satellite i . This weighting scheme ensures that host galaxies that have a large number of satellites (and are hence likely to be more massive than the average host) do not dominate the likelihood. Van den Bosch et al. (2004) compared weighting by host galaxies (the scheme employed here) to weighting by satellite galaxies (which would be equivalent to setting $\lambda = 1$ for all satellites) in simulations and found that the recovered velocity dispersion differs between these two schemes as a function of host luminosity¹¹. Weighting by host galaxy more fairly represents the average mass of host galaxies within a given luminosity or stellar mass bin.

The resulting fit yields not only a measurement of the velocity dispersion but also an estimate of the interloper fraction. Marginalizing the likelihood over η provides an estimate of the 1σ errors on the velocity dispersion.

Redshift uncertainties are accounted for by subtracting in quadrature the rms redshift error, σ_{err} , from the measured velocity dispersion, σ_{los} :

$$\sigma_{\text{est}} = \sqrt{\sigma_{\text{los}}^2 - 2\sigma_{\text{err}}^2}. \quad (4)$$

The redshift uncertainty enters twice because we are subtracting two velocities, the host from the satellite. The resulting velocity dispersion, σ_{est} , is then our best estimate of the true dispersion. For the range of velocity dispersions probed here, folding redshift errors from the DEEP2 and SDSS surveys ($\sigma_{\text{err}} \lesssim 30 \text{ km s}^{-1}$) into our measured dispersion changes results by only a few percent. In the following sections we simplify our notation to $\sigma = \sigma_{\text{est}}$ for brevity.

With an estimate of the velocity dispersion of the host galaxy dark matter halo we can, with additional assumptions, extract the virial mass of the halo. We follow the procedure of Prada et al. (2003) and Conroy et al. (2005b) in converting velocity dispersions to virial masses.

The density profile of a dark matter halo is parameterized using the NFW (Navarro et al. 1997) model:

$$\frac{\rho(r)}{\rho_c^0} = \frac{\delta_c}{(r/r_s)(1+r/r_s)^2} \quad (5)$$

where ρ_c^0 is the present critical density, $r_s = r_{200}/c$, and

$$\delta_c = \frac{200}{3} \frac{c^3}{\ln(1+c) - c/(1+c)}, \quad (6)$$

where r_{200} is defined as the radius where the mean interior density is 200 times the critical density. The concentration, c , is inversely related to the mass of a dark matter halo, and, at fixed mass, scales with redshift as $(1+z)^{-1}$ (Bullock et al. 2001); concentrations for dark matter halos hosting galaxies or clusters range from $3 \lesssim c \lesssim 25$. In our analysis we fix $c = 10$, which is consistent with the concentration of a $\sim 10^{12} h^{-1} M_\odot$ halo at $z = 0$, and scale c by $(1+z)^{-1}$ for higher redshift

¹¹ This is due to the fact that brighter galaxies will have more satellites, especially in a flux limited sample, and hence the difference in weighting schemes is more pronounced in the regime of bright host luminosity.

samples. However, as demonstrated below, the density profile depends only weakly on concentration over the scales probed ($20 \lesssim R_p \lesssim 150 h^{-1} \text{ kpc}$), and hence the assumed concentration has little effect on the resulting mass estimates (cf. Appendix B). Throughout we assume that the satellite galaxies follow the radial profile of the dark matter. The effect of a spatial bias between satellites and dark matter on the recovered mass have been show by van den Bosch et al. (2004) to be at the few percent level (see also Appendix C).

We then determine the radial velocity dispersion profile by integrating the Jeans equation, which relates the density profile and gravitational potential to the radial velocity dispersion, using Equation 5 to specify the potential. Finally, we integrate along the line-of-sight. Both integrations require knowledge of the velocity anisotropy, $\beta \equiv 1 - \sigma_r^2/\sigma_\perp^2$, of the satellite population. Fortunately the line-of-sight velocity dispersion profile depends only weakly on β (van den Bosch et al. 2004; Mamon & Lokas 2005). In Appendix B we explore both an isotropic distribution ($\beta = 0$) and an anisotropy parameterization suggested by Mamon & Lokas (2005), and confirm that the derived mass is robust to assumptions about β . Below we set $\beta = 0$.

Given these assumptions, there remains only one free parameter, the normalization of the dispersion profile, which is related to the mass within r_{200} , denoted M_{200} , of the dark matter halo. The normalization is obtained via χ^2 minimization using the measured $\sigma(R_p)$ points. The majority of the analysis below uses only one velocity dispersion measurement to derive a virial mass. In Appendix B we demonstrate that estimating virial masses with only one dispersion measurement does not bias the recovered mass. Including more velocity dispersion measurements in finer projected separation bins simply has the effect of decreasing the error on the recovered mass (if there are sufficient numbers of satellites to increase the number of radial bins, which is not the case in DEEP2). See Klypin et al. (2006) for a detailed study of the full satellite velocity dispersion profile measured for SDSS host galaxies at $z \sim 0$.

3. THE DATA

This section presents the low- and high-redshift galaxy catalogs used to identify host and satellite galaxies, and describes how to account for the differences in selection effects between the two catalogs.

3.1. The SDSS

The Sloan Digital Sky Survey (SDSS; York et al. 2000; Abazajian et al. 2004; Adelman-McCarthy et al. 2006) is an extensive photometric and spectroscopic survey of the local Universe. As of Data Release 4, imaging data exist over 6670 deg^2 in five bandpasses, u , g , r , i , and z . Approximately 670,000 objects over 4780 deg^2 have been targeted for follow-up spectroscopy as part of SDSS are included in DR4; most spectroscopic targets are brighter than $r = 17.77$ (Strauss et al. 2002). Automated software performs all the necessary data reduction including the assignment of redshifts. Redshift errors are $\lesssim 30 \text{ km s}^{-1}$, similar to DEEP2. The spectrograph tiling algorithm ensures nearly complete sampling (Blanton et al. 2003a), yet the survey is not 100% complete due to several effects: 1) fiber collisions do not

allow objects separated by $< 1'$ to be simultaneously targeted, resulting in $\sim 6\%$ of targetable objects failing to be targeted for spectroscopy; 2) a small fraction ($< 1\%$) of targeted galaxies fail to yield a reliable redshift; and 3) bright Galactic stars block small regions of the sky. None of these effects is expected to impact our analysis. The overall completeness of the SDSS, as defined by the number of objects with successful redshifts divided by the number of objects in the imaging catalog with $r < 17.77$, is $\sim 90\%$. The parent catalog has 166,923 high quality redshifts between $0.01 < z < 0.1$ and $100^\circ < RA < 275^\circ$.

For this analysis we make use of the hybrid NYU Value Added Galaxy Catalog (VAGC) (Blanton et al. 2005). In addition we use the publicly available package `kcorrect v4.1.4` (Blanton et al. 2003b; Blanton & Roweis 2006) to derive restframe B -band magnitudes and $U - B$ colors for SDSS galaxies. All SDSS galaxies are K -corrected to $z = 0.0$. Galaxies are divided into red and blue populations based on the valley visible in the color-magnitude diagram (e.g., Baldry et al. 2004). We account for the fact that the valley moves redward for brighter galaxies with the following color-cut:

$$U - B = -0.066 M_B - 0.05. \quad (7)$$

We also obtain stellar masses for SDSS galaxies using `kcorrect v4.1.4` routines. These stellar masses, which have been obtained assuming a Chabrier IMF, are consistent with the stellar masses of Kauffmann et al. (2003) but are lower by ~ 0.3 dex from the color-based stellar mass estimates of Bell et al. (2003). The offset is due primarily to differences in the assumed IMF.

3.2. The DEEP2 Survey

The DEEP2 Galaxy Redshift Survey (Davis et al. 2003) has gathered optical spectra for $\sim 40,000$ galaxies in the redshift range $0.7 < z < 1.4$ using the DEIMOS spectrograph (Faber et al. 2003) on the Keck II 10-m telescope. The survey spans a comoving volume of $\sim 5 \times 10^6 h^{-3} \text{ Mpc}^3$, covering $\sim 3 \text{ deg}^2$ over four widely separated fields. Target galaxies were selected using BRI imaging from the CFHT telescope down to a limiting magnitude of $R = 24.1$ (Coil et al. 2004). In three of the four fields we also use apparent colors to exclude objects likely to have $z < 0.7$. This pre-selection greatly enhances our efficiency for targeting galaxies at high redshift (Faber et al. 2006). Due to the high spectral resolution ($R \sim 5,000$) and excellent sky subtraction provided by the DEIMOS spectrograph and DEEP2/DEIMOS data reduction pipeline (Cooper et al., in prep), our rms redshift errors are $\sim 30 \text{ km s}^{-1}$ determined from repeated observations. Details of the DEEP2 observations, catalog construction, and data reduction can be found in Davis et al. (2003), Coil et al. (2004), and Davis et al. (2005). Restframe $U - B$ colors and absolute B -band magnitudes have been derived as described in Willmer et al. (2006). The parent DEEP2 catalog includes 21,184 galaxies with high-quality redshifts in the redshift interval $0.70 < z < 1.2$.

Stellar masses for DEEP2 galaxies are estimated in the following way. For the subset of DEEP2 galaxies for which there exists K_s -band imaging, Bundy et al. (2005b) has determined stellar masses based on the methodology outlined in Kauffmann et al. (2003) with

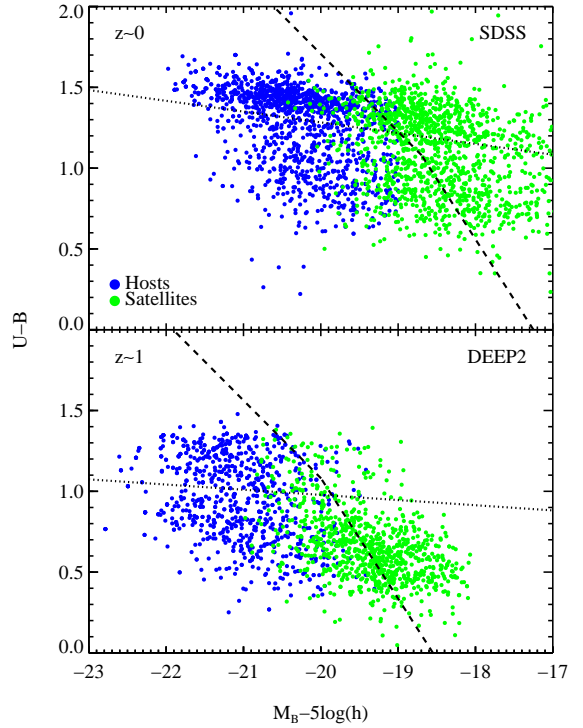


FIG. 1.— Color-magnitude diagram for host galaxies (blue/black points) and satellites (green/grey points). Galaxies drawn from the SDSS at $z \sim 0$ are plotted in the top panel, while the bottom panel shows galaxies at $z \sim 1$ from the DEEP2 survey. The top panel contains only 25% of the total number of objects for clarity. The dashed broken line defines the completeness limit at $z = 1$ (bottom panel), and a similar limit at $z = 0$ (top panel), where in this case the line has been shifted to the right according to the estimated evolution in M_B^* from $z = 1$ to $z = 0$. The dotted line in each panel indicates our division between red and blue galaxies.

a Chabrier IMF. We then use an empirically derived relation between restframe UBV colors and stellar mass (C.N.A. Willmer, private communication) to obtain stellar masses for DEEP2 galaxies that do not have K_s -band imaging. The stellar masses obtained in this way agree well with the stellar mass estimates obtained for DEEP2 galaxies from the `kcorrect v4.1.4` routine (cf. the previous section), as expected since both methods use the same IMF. Since the same IMF is used, we do not expect any systematic offset between the stellar mass estimates at $z \sim 0$ and $z \sim 1$.

As with the SDSS data, DEEP2 galaxies are split into red and blue populations based on the valley in the color-magnitude diagram. These two populations are divided in a manner identical to Willmer et al. (2006) using the following color-cut:

$$U - B = -0.032 (M_B + 21.63) + 1.03. \quad (8)$$

The DEEP2 survey spectroscopically targets $\sim 60\%$ of objects that pass the apparent magnitude and color cuts mentioned above. Of those targeted objects, we are able to secure redshifts for $> 70\%$. Follow-up observations have shown that $\sim 15\%$ of the targets are objects at $z > 1.5$ and fail to yield redshifts from DEEP2 for that reason (C. Steidel, private communication). We therefore have successful redshifts for $60\% \times 85\% = 51\%$ of all galaxies

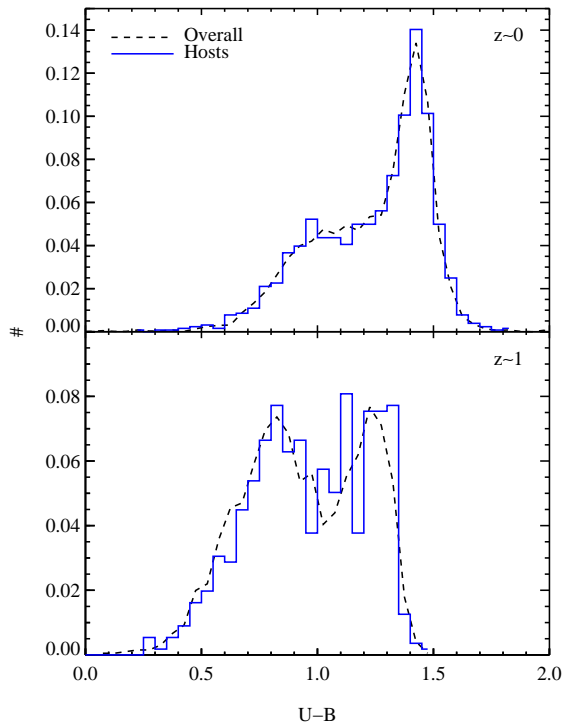


FIG. 2.— $U - B$ colors for host galaxies (solid lines) compared to all galaxies of similar luminosities and redshifts (dashed lines), for galaxies at $z \sim 0$ (top panel) and $z \sim 1$ (bottom panel). The comparison sample was restricted to have the same redshift and luminosity distributions as the host galaxy sample. The histograms are plotted in units such that the integral under each curve is one.

at $0.7 < z < 1.4$ in the surveyed fields with apparent magnitude of $R < 24.1$.

3.3. Defining Uniform Samples from SDSS and DEEP2

Every galaxy survey is unique; unfortunately, that makes comparison between surveys difficult. In our case, there are two separate effects that must be taken into account in order to compare the DEEP2 and SDSS galaxy surveys fairly. The first issue is the differing sampling rates; this is trivial to resolve, however. As mentioned in previous sections, the completeness of the DEEP2 and SDSS surveys are $\sim 50\%$ and $\sim 90\%$, respectively. This difference, if not accounted for, would result in a much larger fraction of falsely isolated host galaxies in the DEEP2 sample (i.e., galaxies that appear isolated in the spectroscopic catalog but are not truly isolated) and could bias the resulting satellite velocity dispersion profile with respect to the SDSS sample.

In order to mitigate this difference we randomly dilute the SDSS redshift catalog to the same completeness as DEEP2 (that is, 40% of SDSS galaxies are randomly removed from the catalog). Extensive tests with mock catalogs have confirmed that for the DEEP2 survey the incompleteness is very close to uniform as a function of 3-dimensional galaxy over-density (Gerke et al. 2005; Cooper et al. 2005), hence this simple random dilution is sufficient for our purposes. As shown in Appendix A, this dilution results in a $\sim 30\%$ increase in the estimated virial masses of host galaxies compared to the complete

(undiluted) SDSS. This should be kept in mind when considering the results in §5.

The second effect primarily impacts the satellite population. While both surveys select targets that are brighter than an *apparent* R -band magnitude limit, in the DEEP2 survey this selection corresponds to an approximately *restframe* B -band selection at $z \sim 0.7$ and approximately *restframe* U -band at $z \sim 1$, while in the SDSS this selection corresponds closely to *restframe* R -band. This means that, for the DEEP2 survey, as one considers fainter objects, redder galaxies will drop out of the survey at a brighter M_B than bluer galaxies. This selection effect is well understood (Willmer et al. 2006), and is accounted for it in the following way.

Figure 1 shows the color-magnitude distribution for all host galaxies (blue/black points) and their associated satellites (red points). Results for host and satellite galaxies at $z \sim 0$ are shown in the top panel, while results for $z \sim 1$ are in the bottom panel. The dotted lines indicate our division into red and blue populations. Note the increase in the number of red host galaxies between $z \sim 1$ and $z \sim 0$ at bright luminosities, where our data are complete. The increasing abundance of red galaxies with time has been studied in detail elsewhere (Bell et al. 2004; Faber et al. 2005; Willmer et al. 2006).

At a specified redshift, the apparent DEEP2 R -band magnitude limit can be modeled by a broken line in the color-magnitude diagram (cf. Figure 1 here and Figure 4 in Willmer et al. (2006); see also Gerke et al. (2006) for a more detailed discussion of this effect). In particular, the broken line in Figure 1 can be used to define a volume limited sample at $z \leq 1$ that uniformly samples color-magnitude space; when selecting such samples we use only DEEP2 galaxies with $z \leq 1$ and include only galaxies that are brighter than this line in color-magnitude space. Note that the broken line is a function of redshift. Moreover, the dearth of faint red galaxies in the bottom panel is attributable to this R -band selection effect. For the sample at $z \sim 0$ the broken line is shifted according to the observed evolution in the B -band luminosity function, $M_B^*(z) = M_B^*(z=0) - 1.37z$, which is approximately independent of color (Faber et al. 2005). Thus, selecting galaxies brighter than this broken line ensures that SDSS and DEEP2 are similarly complete *relative to* M_B^* as a function of both luminosity and color at all redshifts $z \leq 1$.

For host galaxies this selection effect is not particularly important because host galaxies are all rather luminous (by definition, since these galaxies must be bright enough to have satellite galaxies that are at least δM_B magnitudes fainter). For such bright galaxies both very red and very blue host galaxies are included in both surveys over the full redshift ranges we consider. This is apparent in Figure 1, where nearly all of the blue/black points in both panels (representing host galaxies) are to the left of the broken dashed line.

Unfortunately, accounting for the apparent R -band selection effect drastically reduces the number of available satellite galaxies, as can be seen in Figure 1, where most of the green/grey points (representing satellite galaxies) are to the right of the broken dashed line. In order to increase our statistics, when measuring velocity dispersions in §5 we do not account for this selection effect in the manner mentioned above. Assuming that the

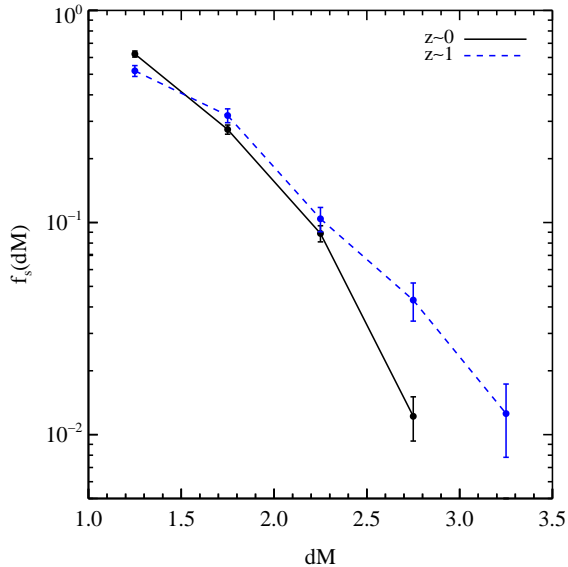


FIG. 3.— Fraction of satellites as a function of $dM \equiv M_B^{\text{sat}} - M_B^{\text{host}}$ in sample A. Satellite-host systems at $z \sim 0$ (solid line) are compared to systems at $z \sim 1$ (dashed line). Selection differences between the parent catalogs from which these systems were extracted are carefully accounted for using the “ R -band cut” (see §3.3 for details).

measured velocity dispersion does not depend on *satellite* properties, then the velocity dispersion should be insensitive to this selection effect, since including this effect will only decrease the total number of host galaxies but will not preferentially select one type of host galaxy (e.g., bright or red) over another¹². However, when comparing host and satellite properties between DEEP2 and SDSS in §4, we account for this selection effect since it strongly impacts the satellite population.

4. PROPERTIES OF HOST GALAXIES AND THEIR ASSOCIATED SATELLITES

In this section we present several salient properties of host and satellite¹³ galaxies and investigate the evolution of these properties from $z \sim 1$ to $z \sim 0$. Differences in the selection effects in DEEP2 and SDSS are taken into account as described in the previous section.

Table 1 lists the different search criteria used for identifying satellites and host galaxies. Our fiducial sample is A; this section and the next contains results using those search criteria only. These search parameters are similar to ones adopted in previous work (McKay et al. 2002;

¹² The situation may not be this simple if host galaxy properties are strongly correlated with satellite properties. For example, if red satellites preferentially exist around red host galaxies, then by missing red satellites we would be implicitly missing red host galaxies. Such a correlation between central and satellite galaxy properties has recently been observed at $z \sim 0$ (Weinmann et al. 2006), though the signal is not large for the types of systems explored here. Indeed, the fraction of red host galaxies does not significantly change when including or neglecting the R -band effect.

¹³ Here we are actually presenting the ensemble properties of true satellites and interloper galaxies. Unless explicitly stated otherwise, we refer to the combination of true satellites and interlopers as “satellites” hereafter.

Prada et al. 2003; Conroy et al. 2005b). In Appendix B, we demonstrate that our results are robust to the particular choice of parameters.

Table 2 contains information on the host and satellite samples using search criteria A. The Table includes the redshift and magnitude ranges over which we search for hosts and satellites, the median redshift of each sample of host galaxies, the number of hosts and satellites found in each sample, and the mean satellite luminosity. This information is tabulated for samples restricted to the region of color-magnitude space where the parent catalogs are complete at both epochs (the samples used in this section, labeled in the table “with R -band cut”), and samples that include regions of color-magnitude space where the parent catalogs are not complete (the samples used in the following section, labeled “without R -band cut” in the table).

In order to quantify the distribution of $U - B$ colors for host galaxies, Figure 2 plots histograms of $U - B$ color at $z \sim 1$ (top panel) and $z \sim 0$ (bottom panel). Each distribution is normalized such that its integral is unity. The sample of host galaxies (solid lines) is compared to an “overall” sample of galaxies (dashed lines). The comparison sample has been constructed such that it samples the redshift-luminosity plane with the same density as the host galaxies. It is evident that host galaxies have a distribution in $U - B$ colors comparable to all galaxies at the same luminosity at both $z \sim 1$ and $z \sim 0$, and that host galaxies at $z \sim 0$ are redder than host galaxies at $z \sim 1$ only insofar as the overall galaxy population is redder at $z \sim 0$ compared to $z \sim 1$. One can also clearly see the growth in the abundance of red galaxies between $z \sim 1$ and $z \sim 0$, as noticed in previous studies (Bell et al. 2004; Faber et al. 2005; Willmer et al. 2006).

The samples used in Figure 2 have the R -band cut taken into account. However, the full samples (neglecting the R -band cut) display nearly identical host $U - B$ color distributions when compared to the R -band cut samples. This indicates that the full samples, which are used in §5, do not contain any *artificial* changes in the $U - B$ color distribution of galaxies with time.

Generating a fair comparison sample is a requisite for interpreting the distribution of colors of host galaxies. Since host galaxies are in general much brighter than an average galaxy (i.e., a galaxy drawn at random from the full survey), without a fair comparison sample we would have falsely concluded that host galaxies are redder than the average galaxy. These selection effects are exacerbated in the DEEP2 sample, where the red galaxy population is a strong function of redshift due both to the apparent R -band limit of the survey and to evolution in red number density, but are effectively mitigated with a proper comparison sample.

Figure 3 plots the distribution, $f_s(dM)$, of magnitude differences, $dM \equiv M_B^{\text{sat}} - M_B^{\text{host}}$ at $z \sim 1$ (dashed line) and $z \sim 0$ (solid line). Error bars denote 1σ Poisson uncertainties. We conclude from these distributions that the average host galaxy at $z \sim 1$ has fainter satellites than an average host galaxy at $z \sim 0$. This conclusion is unchanged if we separately consider $f_s(dM)$ in bins of host galaxy luminosity. The average dM for each sample reflects this difference as well, though less strikingly: at $z \sim 1$ $\langle dM \rangle = 1.60$ while at $z \sim 0$ $\langle dM \rangle = 1.46$.

Note that since these distributions of $f_s(dM)$ are normalized to the total number of satellites at each redshift, these results are insensitive to the presence of interlopers unless interlopers have a dM distribution that varies with redshift. Although such a scenario seems particularly nefarious, it cannot explicitly be ruled out.

In addition we have investigated the sensitivity of these results to our assumed evolution in the luminosity function. Throughout we have assumed that the characteristic scale of the luminosity function evolves as $M_B^*(z) = M_B^*(z=0) - 1.37z$ independent of color (Faber et al. 2005). The evolution in the luminosity function is important here because it determines how the dashed line in Figure 1 evolves with redshift, which in turn defines the samples used in this section. If the amount of evolution in M_B^* is varied by $\pm 0.3z$ (which is the 1σ uncertainty in the evolution of M_B^* as reported by Faber et al. 2005), the qualitative result of Figure 3, namely that DEEP2 satellites are on average fainter with respect to their host luminosities than SDSS satellites, remains unchanged. However, the case of maximal evolution, where M_B^* evolves by 1.67 magnitudes per unit redshift, results in a significantly less striking difference at large dM , for the obvious reason that this maximal evolution in M_B^* allows many more faint satellite galaxies to be included in the sample at $z \sim 0$ (in essence, the dashed line in the top panel of Figure 1 moves to the right). Thus, if the difference in satellite properties seen in Figure 3 is not real, then evolution in M_B^* is even stronger than found by Faber et al. (2005).

Moreover, dynamical friction acting on the $z \sim 1$ host-satellite population would tend to produce a trend *opposite* to what is observed here. Because dynamical friction is most efficient when it acts between objects of comparable mass, it will cause the brightest satellites to sink toward the host preferentially, resulting in comparably *more* fainter satellites at $z \sim 0$ than at $z \sim 1$, contrary to our observations.

In Figure 4 we plot the fraction of host galaxies with at least N_{sat} satellites, $f_s(\geq N_{\text{sat}})$, as a function of N_{sat} , both at $z \sim 1$ (dashed line) and $z \sim 0$ (solid line). Errors reflect Poisson uncertainties. It is evident that, when comparing volume limited samples at $z \sim 1$ and $z \sim 0$ which are similarly complete in color-magnitude space, host galaxies at high redshift are associated with more satellites than host galaxies at low redshift (although the difference is weak, see below). This is illustrated alternatively by considering the average number of satellites per host galaxy: $\langle N \rangle = 1.26$ at $z \sim 1$ and $\langle N \rangle = 1.15$ at $z \sim 0$.

In this case interlopers have a more direct impact. In §5 we show that the interloper fraction decreases from $\sim 21 \pm 6\%$ at $z \sim 1$ to $\sim 16 \pm 4\%$ at $z \sim 0$ (so that within 1σ the interloper fraction is constant with redshift). Therefore, the changes in the average number of satellites per galaxy could be due to changes in interloper contamination with z at $< 1\sigma$. Uncertainties in the evolution of M_B^* from $z \sim 1$ to $z \sim 0$ also strongly impact the results shown in Figure 4 because a larger/smaller evolution in M_B^* than what is assumed here will result in more/less faint galaxies in the $z \sim 0$ “ R -band cut” sample, which will in turn result in more/less satellites at $z \sim 0$ compared to $z \sim 1$. In short, these results are unfortunately too sensitive to various assumptions and

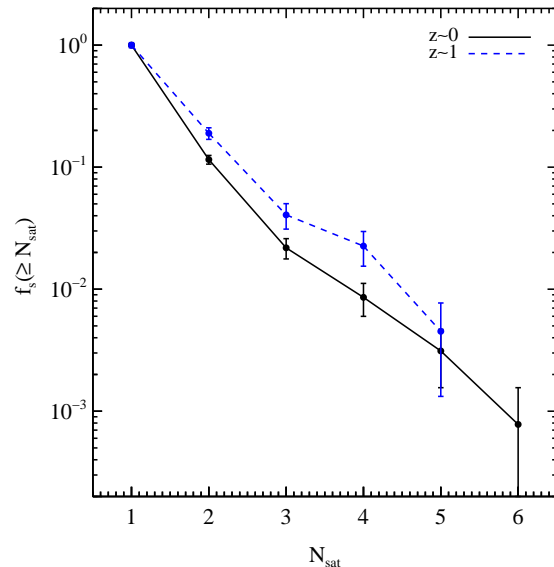


FIG. 4.— Fraction of host galaxies that have $\geq N_{\text{sat}}$ satellites, as a function of N_{sat} . As in the previous figure, we use search criteria A and account for differences between the parent catalogs at $z \sim 1$ and $z \sim 0$ using the “ R -band cut” as described in §3.3.

TABLE 2
SUMMARY OF SAMPLES

	SDSS	DEEP2
redshift range	$0.01 < z < 0.10$	$0.7 < z < 1.2$
$\langle z \rangle$	0.06	0.84
Host $M_B - 5\log(h)$ range	< -19	< -20
<i>without R-band cut:</i>		
Total Sample Size	102,656	21,184
Satellite $\langle M_B - 5\log(h) \rangle$	-18.3	-19.4
N_{sat}	5414	1007
N_{host}	3431	755
<i>with R-band cut:</i>		
Total Sample Size	56,397	12,887
Satellite $\langle M_B - 5\log(h) \rangle$	-19.0	-19.6
N_{sat}	1475	554
N_{host}	1283	440

NOTE. — The host and satellite galaxies contained in these samples were obtained using search criteria A (cf. Table 1). The total sample size for the SDSS survey refers to the survey after it has been diluted by 40% to match the completeness of DEEP2.

uncertainties to provide robust conclusions regarding the differential evolution in satellite numbers between $z \sim 1$ and $z \sim 0$.

5. VELOCITY DISPERSION MEASUREMENTS & DERIVED VIRIAL MASSES

We now present the measured satellite velocity dispersion, σ , as a function of host galaxy redshift, luminosity, stellar mass, and color. In addition, we derive virial mass-to-light ratios (M_{200}/L_B) and virial-to-stellar mass ratios (M_{200}/M_*) at $z \sim 1$ and $z \sim 0$. In this section the R -band selection effect is *not* accounted for when com-

paring samples at $z \sim 1$ and $z \sim 0$; see §3.3 for details. Results are for host and satellite galaxies identified according to search criteria *A* (cf. Table 1). Since both SDSS and DEEP2 are constructed to have the same completeness ($\sim 50\%$), all virial masses quoted herein are $\sim 30\%$ higher than they would be had 100% complete surveys been used. This is attributable to systems that only appear isolated in the diluted sample, but in fact reside within more massive halos with multiple bright companions (see Appendix A).

Appendix B demonstrates that the results presented in this section are robust to various assumptions, including the specific search criteria used to define the samples and the velocity anisotropy and concentration of the satellites orbiting within their host galaxy’s dark matter halo. Appendix C presents an assessment of and motivation for the broader methodological assumptions inherent in using the motions of satellite galaxies to extract host galaxy halo masses.

The nominal redshift limit of the SDSS parent catalog has been extended from $z = 0.1$ to $z = 0.2$ for the highest stellar mass bin, doubling the number of satellites in that bin. Separately measuring the dispersion in this stellar mass bin for the fiducial sample with $z \leq 0.1$ and the extended sample with $z \leq 0.2$ results in differences within 10 km s^{-1} . In other words, adding these higher redshift data does not appear to bias the resulting measurement, but it significantly decreases the errors on the dispersion due to the increased number of satellites. Increasing the redshift limit of the parent catalog for the other samples has little effect since the apparent magnitude limit of the SDSS yields few faint satellite galaxies at higher redshifts.

5.1. Results as a Function of Host Galaxy Luminosity and Stellar Mass

In Figure 5 we present the relative velocity of satellites, dV , as a function of host galaxy stellar mass, M_* , for all satellites within $R_p = [20, 150] h^{-1} \text{ kpc}$ at $z \sim 0$ (top left panel) and $z \sim 1$ (top right panel)¹⁴. Note again that the samples used in this and the following figures do not account for the different survey selection effects between DEEP2 and SDSS (which we argued in §3.3 should not impact the results in this section) and is hence a superset of the samples used in §4. One can see clearly that the satellite velocity dispersion is increasing with increasing host stellar mass. The solid vertical lines indicate the full width at half maximum given by our dispersion measurements, in bins of host stellar mass. The bottom cluster of panels shows the distribution of relative satellite velocities in bins of stellar mass. The smooth lines indicate our best fit Gaussian+constant models for host weighting (solid lines) and satellite weighting (dotted lines). The difference between weighting schemes becomes increasingly important for higher stellar mass bins, since the hosts in these bins have on average more satellites. We only display results as a function of stellar mass for

¹⁴ As we show in Appendix B, the results presented in this section do not change significantly when using larger, smaller, or more bins in R_p . Our fiducial bin size is motivated by the fact that interloper fractions increase with increasing R_p , so although one includes more true satellites with a larger maximum R_p , the larger interloper fraction results in no significant improvement in the dispersion measurement.

TABLE 3
VELOCITY DISPERSIONS AND HALO MASSES OF HOST GALAXIES AS A FUNCTION OF M_B

M_B bin	$\langle M_B \rangle$	color	N_{sats}	σ km s ⁻¹	M_{200}/L_B $h M_\odot/L_\odot$
<i>Results at $z \sim 0$:</i>					
[-19.25, -19.75]	-19.5	all	332	132^{+11}_{-11}	228^{+92}_{-61}
[-19.75, -20.25]	-20.0	all	505	144^{+11}_{-9}	180^{+73}_{-36}
[-20.25, -20.75]	-20.5	all	657	188^{+13}_{-11}	254^{+68}_{-66}
[-20.75, -21.50]	-19.5	all	413	235^{+26}_{-24}	277^{+118}_{-110}
[-19.25, -20.00]	-19.7	red	299	159^{+20}_{-18}	357^{+160}_{-150}
[-20.00, -20.50]	-20.3	red	366	215^{+15}_{-15}	454^{+108}_{-141}
[-20.50, -21.50]	-20.9	red	475	258^{+24}_{-22}	384^{+143}_{-124}
[-19.25, -20.00]	-19.7	blue	267	118^{+11}_{-11}	166^{+56}_{-57}
[-20.00, -20.50]	-20.3	blue	247	139^{+13}_{-11}	143^{+49}_{-44}
[-20.50, -21.50]	-20.8	blue	215	186^{+18}_{-18}	188^{+66}_{-68}
<i>Results at $z \sim 1$:</i>					
[-19.50, -20.75]	-20.4	all	79	118^{+20}_{-18}	71^{+45}_{-37}
[-20.75, -21.50]	-19.5	all	154	153^{+22}_{-20}	63^{+34}_{-29}
[-21.50, -23.00]	-21.9	all	117	272^{+29}_{-40}	130^{+84}_{-51}
[-20.50, -22.00]	-21.3	red	133	231^{+46}_{-37}	151^{+145}_{-79}
[-20.50, -22.00]	-21.2	blue	149	144^{+20}_{-18}	49^{+27}_{-21}

NOTE. — Absolute *B*-band magnitudes, M_B , are quoted as $M_B - 5\log(h)$. Recall that masses and dispersions are *systematically overestimated* (by $\sim 30\%$ in mass) due to incompleteness effects (cf. Appendix A and §3.3).

TABLE 4
VELOCITY DISPERSIONS AND HALO MASSES OF HOST GALAXIES AS A FUNCTION OF M_*

M_* bin	$\langle M_* \rangle$	N_{sats}	σ km s ⁻¹	$M_{200}/M_* h$
<i>Results at $z \sim 0$:</i>				
[9.8, 10.4]	10.2	422	118^{+9}_{-9}	105^{+27}_{-31}
[10.4, 10.7]	10.6	659	155^{+11}_{-9}	83^{+32}_{-35}
[10.7, 11.0]	10.8	663	197^{+15}_{-15}	81^{+36}_{-19}
[11.0, 11.5]	11.1	483	423^{+59}_{-48}	333^{+146}_{-155}
<i>Results at $z \sim 1$:</i>				
[9.6, 10.4]	10.1	74	109^{+22}_{-15}	69^{+61}_{-35}
[10.4, 11.0]	10.7	153	162^{+24}_{-20}	57^{+29}_{-28}
[11.0, 11.6]	11.2	121	290^{+31}_{-40}	77^{+46}_{-30}

NOTE. — All stellar masses, M_* , are quoted in units of $\log(M_* h^{-2} M_\odot)$. Recall that masses and dispersions are *systematically overestimated* (by $\sim 30\%$ in mass) due to incompleteness effects (cf. Appendix A and §3.3).

simplicity, but we also fit for σ in bins of M_B .

Figure 6 contains our main results. The top panels present the satellite velocity dispersion measured within a projected separation of $R_p = [20, 150] h^{-1} \text{ kpc}$ as a function of *B*-band magnitude (top left panel) and stellar mass (top right panel) for galaxies at $z \sim 1$ (blue diamonds) and $z \sim 0$ (black circles). The 1σ errors on

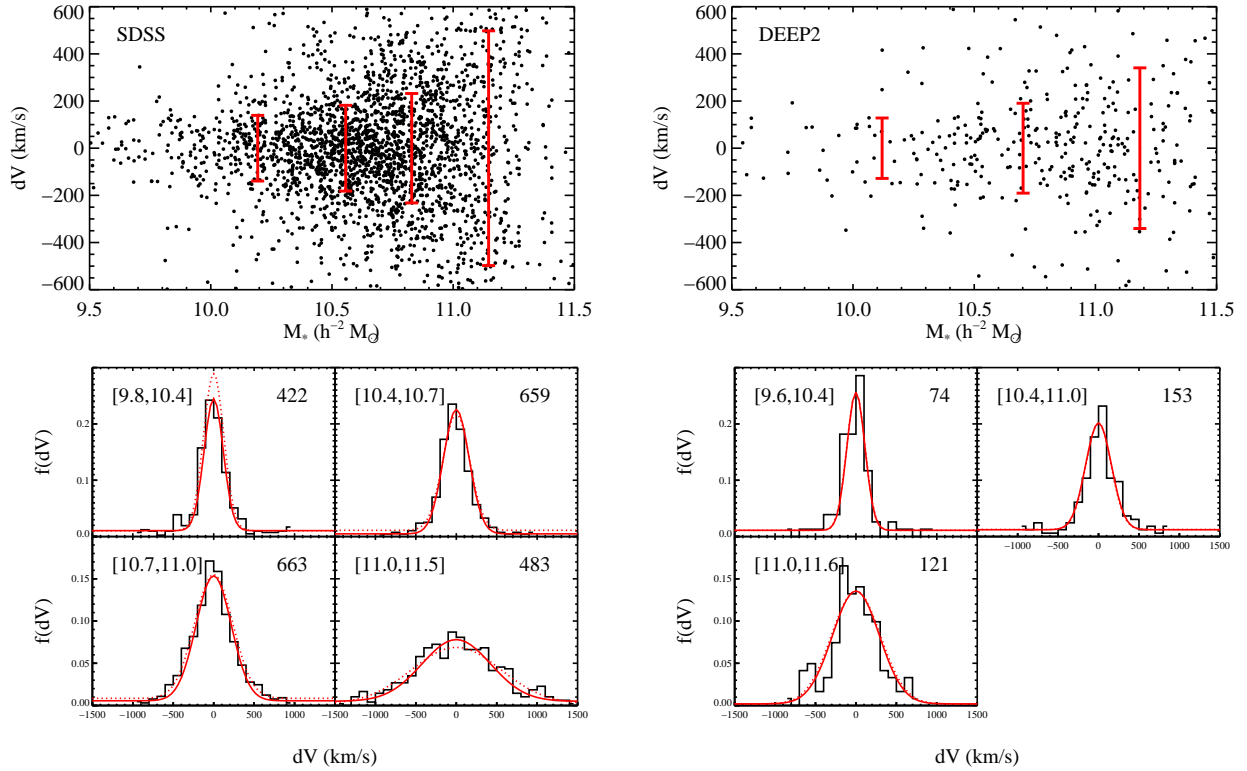


FIG. 5.— *Left panels:* The top panel plots the relative line-of-sight satellite velocity, dV , as a function of host stellar mass, M_* , for all satellites within $R_p = [20, 150] h^{-1}$ kpc at $z \sim 0$ from sample *A*. The solid vertical lines indicate the full width at half maximum taken from the measured dispersion within four bins in host stellar mass. The bottom panels display the dV distribution in bins of stellar mass normalized to the total number of satellites within the bin (stellar mass bin width is displayed in the top left corner in units of $\log(M_* h^{-2} M_\odot)$). The top right corner notes the number of satellites within each bin. We over-plot the best fit Gaussian+constant model weighted by host galaxy (used in the following analysis; *solid lines*) and weighted by satellite galaxy (*dotted lines*). *Right panels:* Same as the left panels, now for data at $z \sim 1$.

the dispersion measurement were obtained from the likelihood contours described in §2.2 and error bars in the B -band magnitude on the x -axis represent the 68% range within each magnitude bin. The information in these figures is also listed in Tables 3 and 4 where we list, for each bin in host M_B and M_* , the number of satellites, mean M_B and M_* of host galaxies, recovered satellite velocity dispersions, and virial-to-stellar mass and mass-to-light ratios.

In the bottom panels we present the same information, where now the velocity dispersion measurements have been converted into virial masses (cf. §2.2) and quote our results in terms of the virial mass-to-light ratio (M_{200}/L_B , bottom left panel) and the virial-to-stellar mass ratio (M_{200}/M_* , bottom right panel). Note that in order to convert the velocity dispersion into a virial mass we use only the velocity dispersion within $R_p = [20, 150] h^{-1}$ kpc rather than attempting to measure the dispersion in multiple bins; this is due to our limited statistics, especially at $z \sim 1$.

Errors on the virial mass-to-light ratios reflect the errors on the virial mass, which were obtained from χ^2 minimization between the observed velocity dispersion and the theoretical dispersion profile. Any errors in the luminosity are not included when calculating the error on M_{200}/L_B ; we simply use the mean luminosity within

each bin (the median B -band magnitude agrees with the mean to within ± 0.01). Error bars on the B -band magnitudes on the x -axis again represent the 68% range in each magnitude bin. The virial-to-stellar mass ratios are plotted similarly.

We mention in passing that the mean redshift of host galaxies does not vary strongly across the B -band magnitude and stellar mass bins. At $z \sim 0$ the mean redshift varies from 0.044 in the faintest bin to 0.076 in the brightest bin, while at $z \sim 1$ it increases from 0.80 to 0.91 between the faintest to brightest magnitude bins explored here.

In addition to velocity dispersion measurements, our maximum-likelihood technique provides an estimate of the interloper fraction (the number of interlopers divided by the total number of satellites) for each sample. The interloper fraction for the $z \sim 0$ samples is $\sim 16 \pm 4\%$ and is constant (within 1σ) across the host luminosity and stellar mass bins. This interloper fraction at $z \sim 0$ is in agreement with previous work. In particular, Prada et al. (2003) found interloper fractions of 17–20% depending on their sample definition. At $z \sim 1$ the interloper fractions are noisier due to the smaller number of satellites. We measure an average interloper fraction at $z \sim 1$ of $\sim 21 \pm 6\%$, again with little variation across the luminosity and stellar mass bins. While the interloper fractions at both $z \sim 0$ and $z \sim 1$ are consistent within

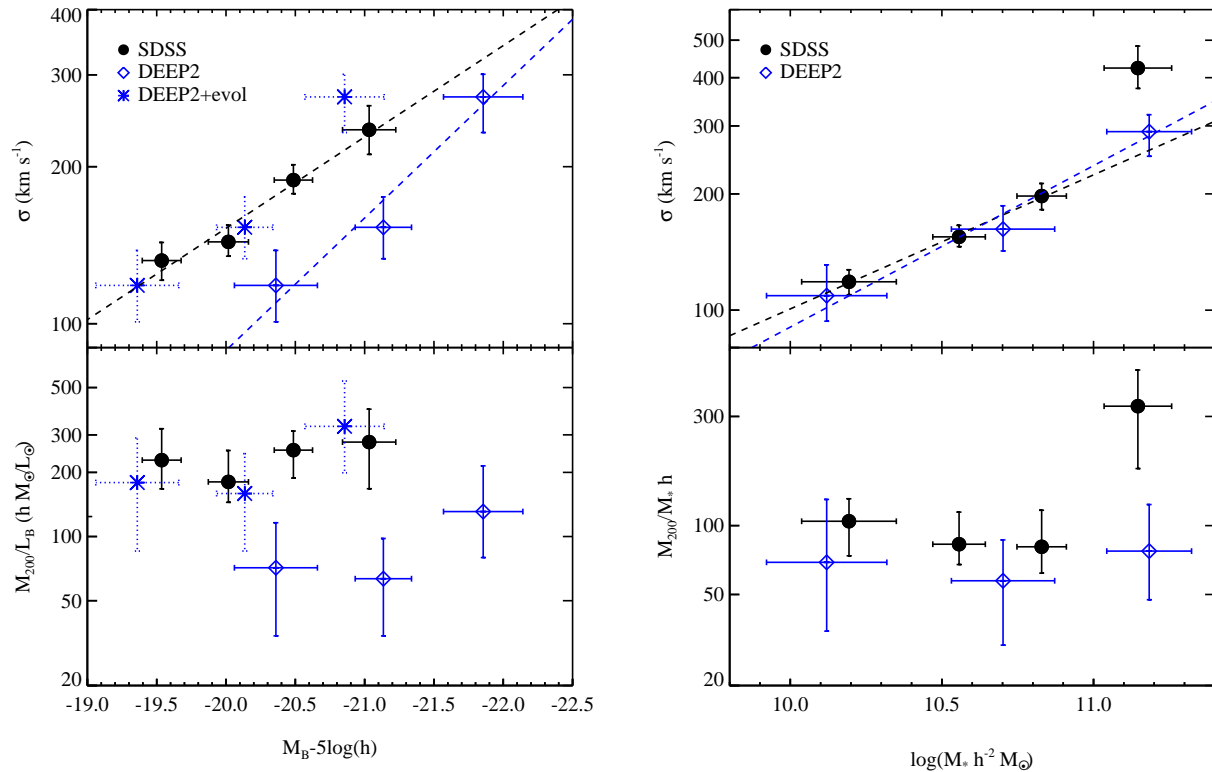


FIG. 6.— *Top panels*: Satellite velocity dispersion, measured within $R_p = [20, 150] h^{-1}$ kpc, for host galaxies at $z \sim 1$ (*diamonds*) and $z \sim 0$ (*circles*) from sample A. In the left panel we plot the dispersion as a function of the B -band absolute magnitude of the host galaxy, while the right panel is as a function of stellar mass (M_*). In addition we show the $z \sim 1$ measurements modified by a one magnitude dimming in the B -band luminosity of host galaxies (*stars*). The dashed lines are from Equations 9 and 10. *Bottom left panel*: Mass-to-light ratios as a function of host galaxy M_B . *Bottom right panel*: Virial-to-stellar mass ratio as a function of host galaxy stellar mass. Since virial mass is defined with respect to the redshift-dependent critical density, an increase in M_{200}/M_* of 1.3 is expected for an intrinsically non-evolving $M_{200}/M_* - M_*$ relation (the same is true as a function of M_B). Symbol types are the same as the top panels.

1σ , $z \sim 1$ host galaxies do have a slightly higher fraction of interlopers than $z \sim 0$ hosts. A higher interloper rate at higher redshift might be attributable to the fact that more systems were still in the process of assembling then, and hence the higher fraction of interlopers could be reflecting a higher fraction of systems that have not yet settled into dynamical equilibrium. Such a trend should not bias our velocity dispersion and mass estimates because the interlopers are effectively accounted for in the dispersion measurements, regardless of their fraction.¹⁵

Figure 6 includes power-law fits to the observed $\sigma - L_B$ and $\sigma - M_*$ relations:

$$\sigma \propto \begin{cases} L_B^{0.4}, & z \sim 0 \\ L_B^{0.6}, & z \sim 1, \end{cases} \quad (9)$$

$$\sigma \propto \begin{cases} M_*^{0.4}, & z \sim 0 \\ M_*^{0.4}, & z \sim 1, \end{cases} \quad (10)$$

¹⁵ These interloper fractions are likely underestimated because we have assumed that interlopers are distributed uniformly in dV while tests based on mock galaxy catalogs suggest that the interloper distribution is more complex (van den Bosch et al. 2004; Chen et al. 2005). Based on tests with mock catalogs, van den Bosch et al. (2004) found that the assumption of a constant distribution of interlopers underestimates the interloper fraction by as much as 50%. Note, however, that these details do not impact the recovered satellite velocity dispersion and will affect the interloper fractions at $z \sim 1$ and $z \sim 0$ in the same way.

with 1σ errors on the exponents of 0.1. We use only the lower three $\sigma(M_*)$ points for the fit at $z \sim 0$ because the dispersion in the highest stellar mass bin seems to deviate strongly from the relation indicated by the other points. Although the $\sigma - L_B$ relation at $z \sim 1$ is formally steeper than the corresponding relation at $z \sim 0$, we emphasize that the two slopes are consistent with one another, and stress that the inferred slope of the $\sigma - L_B$ relation depends on the range of luminosities probed and hence the exponents in this relation should in general be treated with caution (the same can be said of the $\sigma - M_*$ relation).

For an NFW density profile with no anisotropy, virial mass is related to velocity dispersion as $M_{200} \propto \sigma^{2.5}$ at $R_p = 100 h^{-1}$ kpc (which is roughly the mean satellite R_p used in our analysis), and thus $M_{200}/L_B \propto \sigma^{2.5}/L_B$. Hence, at $z \sim 0$, Equation 9 implies that $M_{200}/L_B \propto L_B^{2.5 \times 0.4 - 1} \sim \text{constant}$, while at $z \sim 1$ $M_{200}/L_B \propto L_B^{0.5 \pm 0.3}$. Notice that in general, if $\sigma \propto L^\alpha$, M/L will increase with L only when $\alpha > 0.4$. Similar equations can be derived as a function of host galaxy stellar mass. These inferred M_{200}/L_B versus L_B trends are perfectly consistent with the observed trends in the bottom panels of Figure 6. In addition, the slope of our measured $\sigma - L_B$ relation at $z \sim 0$ is consistent with previous estimates from satellite dynamics (McKay et al.

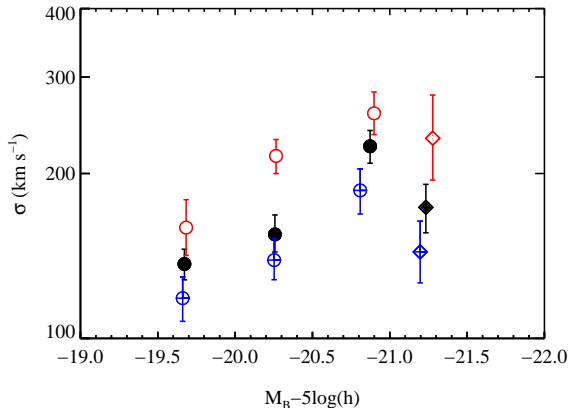


FIG. 7.— Satellite velocity dispersion as a function of host galaxy $U - B$ color and M_B for samples at $z \sim 0$ (circles) and $z \sim 1$ (diamonds). At fixed M_B there is a clear difference between all (solid, black), red (open red), and blue (open with crosses, blue) hosts both at $z \sim 1$ and $z \sim 0$.

2002; Prada et al. 2003; Brainerd 2005).

One should keep in mind that the $\sigma - L_B$ and $\sigma - M_*$ relations are not directly comparable because a bin in L_B contains a different fraction of red host galaxies from a similar bin in stellar mass. This is due to the fact that stellar mass is much more strongly correlated with galaxy color than B -band absolute magnitude. At $z \sim 0$ the fraction of host galaxies with red $U - B$ color increases from 48% to 77% in our lowest to highest B -band magnitude bins, while the red fraction increases from 26% to 91% from the lowest to highest stellar mass bins. Similarly, at $z \sim 1$ the fraction of red host galaxies increases from 33% to 55% from the faintest to brightest B -band magnitude bin, and from 4% to 88% for the smallest to largest stellar mass bins. The strongly varying fraction of red host galaxies as a function of host stellar mass makes the comparison and interpretation of the evolution in $\sigma(M_*)$ between $z \sim 1$ and $z \sim 0$ simpler because each end of the $\sigma - M_*$ relation is dominated by a single population (red galaxies at the massive end and blue galaxies at the faint end).

The $\sigma - M_*$ and $M_{200}/M_* - M_*$ relations show little evolution between $z \sim 1$ and $z \sim 0$ except for the highest stellar mass bin. For host galaxies with $M_* \lesssim 10^{11} h^{-2} M_\odot$ the raw increase in M_{200}/M_* is constrained to 1.4 ± 0.9 (but see below). For host galaxies with larger stellar mass the virial-to-stellar mass ratio increases by a factor of 4 ± 3 between these epochs. These hosts have large dispersions ($\gtrsim 300 \text{ km s}^{-1}$) that correspond to massive dark matter halos ($> 10^{13} h^{-1} M_\odot$), which commonly contain groups of galaxies, and hence they probably should not be interpreted in the same way as less massive host galaxies. We defer a more detailed discussion of this extreme population to §7.2.

When interpreting the evolution in the virial mass-to-light ratio, one should keep in mind that our *definition* of mass changes with redshift since the critical density is redshift-dependent. Specifically, at a fixed velocity dispersion, the virial mass defined according to a region enclosing a mean density 200 times the critical density, M_{200} , *increases* by a factor of ~ 1.3 from $z \sim 1$ to $z \sim 0$.

A changing virial mass with redshift, even for a static, intrinsically non-evolving dark matter halo (i.e., a halo that is not accreting new material), is a generic feature of all common virial definitions. In other words, an increase in M_{200}/M_* of 1.3 between $z \sim 1$ and $z \sim 0$ is expected for an intrinsically non-evolving $M_{200}/M_* - M_*$ relation.

Such an increase is precisely what is observed for host galaxies with $M_* \lesssim 10^{11} h^{-2} M_\odot$, which show a raw increase in M_{200}/M_* of 1.4 ± 0.9 . Hence even this small increase does not reflect physically interesting changes in host galaxies. Folding in the changing virial definition with redshift results in an “intrinsic” increase in M_{200}/M_* of only 1.1 ± 0.7 . This differentiation between intrinsic and definitional changes in M_{200}/M_* is supported by the $\sigma - M_*$ relation for host galaxies, which displays a very small raw increase from $z \sim 1$ to $z \sim 0$ for hosts with $M_* \lesssim 10^{11} h^{-2} M_\odot$. Below, the intrinsic growth in M_{200}/M_* with time will refer to growth after removing the factor of 1.3.

To facilitate comparisons between $z \sim 1$ and $z \sim 0$, in the left hand panels of Figure 6 we additionally plot the satellite velocity dispersion and M_{200}/L for galaxies at $z \sim 1$ where all M_B values have been dimmed by one magnitude to account for evolution in M^* between the median redshifts of the two samples ($= 1.37 \times (0.84 - 0.06)$; cf. Faber et al. 2005). This brings the two samples into near agreement. Our results as a function of M_B are thus consistent with host galaxies at $z \sim 1$ *evolving into* host galaxies at $z \sim 0$ if their luminosities on average dim by one magnitude and their dark matter halo masses do not grow between these epochs. However, we emphasize that since this interpretation neglects the growth of dark matter halos with time it is rather unrealistic, and return to a more detailed interpretation of these results in §7.2.

5.2. Results as a Function of Host Galaxy Color

Finally, we investigate the $\sigma - L_B$ relation as a function of host galaxy $U - B$ color. The $\sigma - M_*$ relation cannot be probed as a function of color because the high/low stellar mass bins are almost entirely dominated by red/blue galaxies, so it is impossible to separate the host population into red and blue at these extremes of the stellar mass distribution and obtain adequate statistics, but these effects are more modest for σ vs. M_B . Figure 7 and Table 3 present the satellite velocity dispersion as a function of host galaxy luminosity, color, and redshift. We can only probe one broad bin in host luminosity ($-20.5 < M_B - 5 \log(h) < -22.0$) at $z \sim 1$ due to the limited number of satellites available. For every bin in host B -band absolute magnitude there is a clear dependence of satellite velocity dispersion on host $U - B$ color, at both $z \sim 1$ and $z \sim 0$.

6. COMPARISON TO A SEMI-ANALYTIC MODEL

We now compare our results to predictions from a semi-analytic model (SAM) of galaxy formation based on the Millennium Run (MR) N -body simulation (Springel et al. 2005), which is described in detail in Croton et al. (2006). In brief, the model evolves the contents of dark matter halos self-consistently according to a set of simple physical prescriptions derived from observational and theoretical phenomenology that govern the evolution of baryons in a cosmological setting. These prescriptions track a wide range of physics, in-

cluding the cooling of baryons, star-formation in galactic disks and merger induced starbursts, supernova and AGN feedback, the tidal stripping of gas, and black hole growth. This model matches an array of observational results at $z \sim 0$, including the b_j - and K -band galaxy luminosity functions and the color bimodality visible in the color-magnitude relation.

In order to facilitate direct comparison to our observational results, mock surveys have been constructed out of the MR that match the geometry and sampling rates of both the DEEP2 and SDSS surveys. We then apply exactly the same search criteria and analysis methods to these mock surveys as to the data.

Figure 8 presents a comparison of M_{200}/M_* between the MR SAM and data at $z \sim 0$ (*top panel*) and $z \sim 1$ (*bottom panel*)¹⁶. The $M_{200}/M_* - M_*$ relations for MR host galaxies have shapes quite similar to the observed relations at both low and high redshift (note that the highest stellar mass bin at $z \sim 1$ in the MR has only 13 satellites and hence that measurement is unstable). In addition, the normalization of this relation in the MR is in agreement with observations at $z \sim 1$, though systematically lower compared to observations at $z \sim 0$. This qualitative agreement highlights the power of current generation N-body simulations, including the MR, which explicitly follow sub-structure within each virialized dark matter halo. Such sub-structures host the population of satellite galaxies from which our analysis is derived, and are clearly important for accurate modeling of the internal dynamics of group and cluster systems.

The MR also provides an explicit test of our methodology since we can compare the halo mass inferred from satellite kinematics to the true average host dark matter halo mass, which is readily available from the MR. The good agreement in Figure 8 between the true and satellite-derived masses is very encouraging, though not unexpected based on previous tests of the satellite methodology (cf. Appendix C). The agreement is less than ideal at the highest stellar mass bins at both $z \sim 1$ and $z \sim 0$, though at $z \sim 1$ the discrepancy is of limited significance due to the modest number of pairs in the MR in that bin.

At $z \sim 0$ the discrepancy between true and satellite-derived halo masses is potentially more interesting. At this late epoch the MR SAM contains many satellites whose host subhalos have been stripped below the resolution limit of the simulation (the so-called ‘‘orphan’’ population). In this situation the MR implements a prescription for the dynamical evolution of such galaxies rather than tracking its evolution explicitly with the subhalo. When such galaxies are removed from the MR, the agreement between true and satellite-derived masses in the two highest stellar mass bins at $z \sim 0$ significantly improves while simultaneously preserving the agreement at lower stellar masses and higher redshift. This issue clearly warrants further study.

7. DISCUSSION

7.1. Compatibility with Weak Lensing Results

¹⁶ The MR galaxy formation model was run with a Salpeter IMF; in order to compare to the observational stellar masses, which were computed with a Chabrier IMF, the MR stellar masses have been lowered by the known offset between these IMFs, 0.3dex.

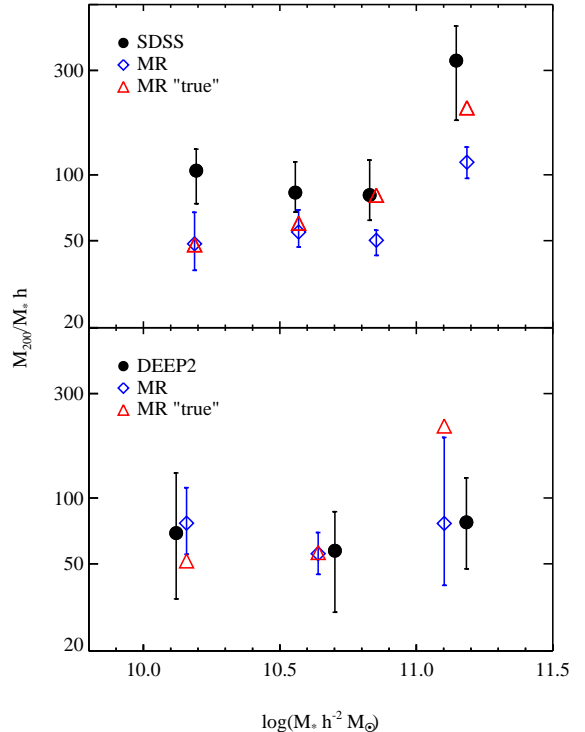


FIG. 8.— Observed and predicted virial-to-stellar mass ratios, M_{200}/M_* , at $z \sim 0$ (*top panel*), and $z \sim 1$ (*bottom panel*). The observed virial-to-stellar mass ratios (*circles*) are compared to both the true average virial-to-stellar mass ratio (*triangles*) in the MR semi-analytic model and the ratio derived from applying our satellite kinematics measurement techniques to that sample (*diamonds*).

Our results at $z \sim 0$ are most directly comparable to the weak lensing results of Hoekstra et al. (2005) who measured the lensing signal around a sample of isolated galaxies observed by the Red-Sequence Cluster Survey. They found that $M_{\text{vir}}/L \propto L^{0.5}$ for isolated galaxies brighter than $M_B - 5\log(h) = -20.0$, and $M_{\text{vir}}/L \sim \text{constant}$ for fainter galaxies. Our results in Figure 6 are consistent with these findings. In particular, note that our derived M_{200}/L_B appears to flatten out at $M_B \lesssim -20.0$, and we find a best-fit power law exponent of 0.5 for M_{200}/L_B versus L_B for the three data points brighter than $M_B = -20.0$ (though taken together, our data are consistent with a slope of 0.0). As discussed in Hoekstra et al. (2005), their results are in broad agreement with other weak lensing studies. This overall consistency is quite encouraging since these two methods for deriving virial masses are almost entirely independent.

In addition there is rough agreement in the normalization of the relations derived from the two techniques. Hoekstra et al. (2005) found $M_{\text{vir}} = 1.9 \times 10^{12} h^{-1} M_\odot$ for galaxies with luminosity $M_B - 5\log(h) = -20.6$ at $z = 0.32$. In order to compare our results to theirs, we have evolved our absolute magnitudes by $1.37z$ to their median redshift, converted our definition of mass to theirs (their definition of virial mass is a region that encloses a mean density Δ_{vir} times the mean density of the universe, where $\Delta_{\text{vir}} = 337$ at $z = 0$ and varies with redshift), and corrected for the $\sim 30\%$ over-prediction in

our derived mass due to incompleteness (cf. Appendix A). With these corrections we find a virial mass of $M_{\text{vir}} = 1.8 \times 10^{12} h^{-1} M_{\odot}$ for host galaxies with a mean absolute magnitude $M_B - 5\log(h) = -20.4$. While this agreement is encouraging, at lower luminosities our corrected masses tend to be higher than those quoted in Hoekstra et al. (2005), by about 40% (though they still agree within 2σ).

Mandelbaum et al. (2006, M05) measured the average virial-to-stellar mass ratio for galaxies in the SDSS as a function of galaxy stellar mass and found that $M_{200}/M_* = 37 \pm 13 h$ ($47 \pm 14 h$) for early-type galaxies with $\log(M_*) = 10.5(10.7) h^{-2} M_{\odot}$ (confidence levels quoted in M05 are 95%). In the present work we find $M_{200}/M_* = 64^{+25}_{-12} h$ ($62^{+28}_{-15} h$) for host galaxies with $\log(M_*) = 10.6(10.8) h^{-2} M_{\odot}$, at $z \sim 0$ (after correcting for the $\sim 30\%$ overestimate in our masses due to incompleteness; cf. Appendix A). Our results are hence quite consistent with M05 at the 95% confidence level. In addition, including the stellar mass of satellites results in a virial-to-stellar mass ratio of the entire system for $(M_{200}/M_*)_{\text{tot}} = 52^{+20}_{-9} h$ for host-satellites systems with $\log(M_{*,\text{tot}}) = 10.6 h^{-2} M_{\odot}$.

Perhaps most importantly, our results agree with M05 in the highest stellar mass bin. For host galaxies with $\log(M_*) = 11.1 h^{-2} M_{\odot}$ we find $M_{200}/M_* = 256^{+122}_{-119} h$ (again corrected for the $\sim 30\%$ overestimate in M_{200}) while M05 found $M_{200}/M_* = 284^{+49}_{-75} h$ for early-type galaxies with mean stellar mass $\log(M_*) = 11.3 h^{-2} M_{\odot}$.

Most recently, Heymans et al. (2006, H06) measured the weak lensing signal for galaxies in the COMBO-17 and GEMS surveys. These authors found that the virial-to-stellar mass ratio decreases from $z \sim 0.8$ to $z \sim 0$ by at most a factor of 2.6 (1σ confidence) and are consistent with a constant value of $M_{200}/M_* = 66^{+15}_{-20} h$ over this redshift range. These authors include only galaxies with $\log(M_*) > 10.2 h^{-2} M_{\odot}$, where there data is complete for $z < 0.8$. The evolution of M_{200}/M_* measured in the present work is again in good agreement with these weak lensing results, including the non-evolving virial-to-stellar mass ratio from $z \sim 1$ to $z \sim 0$ for galaxies with $M_* \lesssim 10^{11} h^{-2} M_{\odot}$ (the average stellar mass of galaxies in H06 is $\langle \log(M_*) \rangle = 10.5 h^{-2} M_{\odot}$).

A more detailed comparison between these two methods for estimating halo masses is complicated because the systems that satellite dynamics probe are systematically different from the systems weak-lensing analyses explore. In order to uncover any measurement bias one would need to measure the weak-lensing signal for the same set of galaxies that are used in satellite dynamics studies, which is likely feasible given the current number of host galaxies found in the SDSS.

7.2. The Evolution of Host Galaxies from $z \sim 1$ to $z \sim 0$

We now explore the evolution in the virial mass-to-light and virial-to-stellar mass ratios – i.e., M_{200}/L_B and M_{200}/M_* , respectively – between $z \sim 1$ and $z \sim 0$. Evolution in M_{200}/M_* is somewhat simpler to interpret because stellar mass can only increase with time, and so we consider it first.

Our data suggest a *bimodality* in the evolutionary history of host galaxies between $z \sim 1$ and $z \sim 0$: host galaxies below $M_* \sim 10^{11} h^{-2} M_{\odot}$ maintain a roughly

constant virial-to-stellar mass ratio (the intrinsic ratio increases by a factor of 1.1 ± 0.7) while hosts above this stellar mass scale, which are predominantly red in $U - B$ color, experience a factor of 4 ± 3 increase in M_{200}/M_* . The quenching of star formation, which becomes particularly effective above this stellar mass (Dekel & Birnboim 2006; Croton et al. 2006; Cattaneo et al. 2006), is a key physical process likely responsible for this bimodality.

Galaxies below $M_* \sim 10^{11} h^{-2} M_{\odot}$ continue to form stars between $z \sim 1$ and $z \sim 0$. Recent modeling of the star formation history of relatively low-mass blue galaxies has suggested that these objects grow in stellar mass by roughly a factor of 2 between these epochs (Noeske et al. 2006). Cosmological simulations of dark matter reveal that $\sim 10^{12} h^{-1} M_{\odot}$ dark matter halos – such as the ones which our typical host galaxies appear to reside in – grow on average by a factor of ~ 2 over this time period (Wechsler et al. 2002). The growth in stellar mass of host galaxies hence proceeds in lockstep with the growth of their dark matter halos, yielding a constant virial-to-stellar mass ratio from $z \sim 1$ to $z \sim 0$.

If the virial-to-stellar mass ratio for these galaxies does not change with z , their star formation efficiency must also remain constant over this time. Specifically, after correcting for the $\sim 30\%$ overestimate in our masses due to incompleteness (cf. Appendix A), our results imply a star formation efficiency for host galaxies of $\eta \equiv \frac{M_* \Omega_m}{M_{200} \Omega_b} \approx 0.13$, assuming a universal baryon fraction of 0.17 (Spergel et al. 2006) and $h = 0.7$. Including the stellar mass of the satellite galaxies yields an efficiency for the entire system of $\eta \approx 0.16$. These efficiency factors are bracketed by values of $\eta = 0.08$ derived from the global baryonic mass function (Read & Trentham 2005) and various weak-lensing studies, which find $\eta \approx 0.05 - 0.3$ (Mandelbaum et al. 2006; Heymans et al. 2006).

The lack of evolution in M_{200}/M_* found here is broadly consistent with measurements of the evolution of the stellar mass Tully-Fisher relation (TFR) over this time period. In particular, Conselice et al. (2005) and Boehm & Ziegler (2006) converted their stellar mass TFR into a dynamical-to-stellar mass ratio and found little evolution from $z \sim 1$ to $z \sim 0$; using ~ 550 galaxies, Kassin et al. (2006a) found no evolution in the stellar mass TFR between these epochs, which under simple assumptions translates into a non-evolving dynamical-to-stellar mass ratio. One should keep in mind that there are numerous details which make a one-to-one comparison between the stellar mass TFR and our results complicated. For example, the relation between internal galaxy kinematics (e.g. the maximum circular velocity of the disk) and dark matter halo kinematics is non-trivial, and likely changes with time. Recent SPH simulations of individual disk galaxies have found that stellar mass and circular velocity co-evolve (both roughly doubling between $z \sim 1$ and $z \sim 0$), yielding a non-evolving stellar mass TFR (Portinari & Sommer-Larsen 2006).

The evolutionary history of the most massive ($M_* \gtrsim 10^{11} h^{-2} M_{\odot}$, and therefore red) host galaxies is predicted to be qualitatively different. A variety of recent models suggest that feedback mechanisms in high mass halos prevent the ambient gas from cooling and forming new stars (Cattaneo et al. 2006; Dekel & Birnboim 2006; Croton et al. 2006). Hence the stellar mass of these

galaxies can only increase via merging with other galaxies. Numerous observational results suggest that the stellar mass in bright red galaxies *at most* doubles since $z \sim 1$ (Borch et al. 2006; Bundy et al. 2005a; Bell et al. 2004). Yet massive dark matter halos are growing rapidly between $z \sim 1$ and $z \sim 0$ (Wechsler et al. 2002). The quenching of star formation within these dark matter halos provides a natural, qualitative, explanation for the observed growth in M_{200}/M_* with time.

The quenching of star formation in these massive systems implies that their star formation efficiency decreases with time since new gas that comes into these halos is prevented from condensing to form new stars. The observed increase in M_{200}/M_* between $z \sim 1$ and $z \sim 0$ for these systems corresponds to a decrease in efficiency from 14% to 3% between these epochs.

This simple picture is complicated by our selection criteria. In particular, host galaxies are required to not have any comparably bright companions within a search cylinder. This non-trivial selection makes it difficult to reason generally about the growth of halos and stellar mass with time, and favors comparisons to more detailed models of galaxy formation (see §6 and below). However, these selection effects may also account for part of the observed increase in M_{200}/M_* between $z \sim 1$ and $z \sim 0$.

Due to the continual merging of galaxies within halos over time, galaxies can enter the host galaxy sample between $z \sim 1$ and $z \sim 0$. In particular, objects within groups and clusters of galaxies at $z \sim 1$, which are in halos that are more massive than the average host galaxy dark matter halo, may not be classified as host galaxies due to their bright companions, but can *turn into* what we would call host galaxies at late times. As groups and clusters at $z \sim 1$ evolve, dynamical friction will cause some fraction of bright companion galaxies to merge with the central galaxy. Those systems in which only one luminous galaxy remains within a massive dark matter halo will be similar to so-called “fossil groups” (see e.g. Jones et al. 2003). The increase of fossil groups between $z \sim 1$ and $z \sim 0$ is a possible explanation for the increase in M_{200}/M_* for high-stellar-mass host galaxies. This mechanism will likely not affect the evolution of M_{200}/M_* at smaller host stellar masses because the merging of $\sim L^*$ galaxies in massive halos will generate massive red galaxies (Hopkins et al. 2006), not lower-mass, blue galaxies.

The stellar mass and redshift dependence of the virial-to-stellar mass ratio of host galaxies is reproduced qualitatively in the Millennium Run semi-analytic model (Croton et al. 2006). In particular, this model manages to capture the stellar mass dependence of M_{200}/M_* at $z \sim 1$ quite well. At $z \sim 0$ this model reproduces the observed *shape* of the $M_{200}/M_* - M_*$ relation, though with a lower normalization. The Millennium Run, and models like it, are particularly useful for interpreting these results because these semi-analytic models track the *evolutionary history* of mock galaxies. Hence, for example, we are capable of directly confronting the explanations presented above with a self-consistent model. We can ask where host galaxies at $z \sim 1$ end up at $z \sim 0$ and, conversely, where $z \sim 0$ host galaxies were at $z \sim 1$. Such a comparison will be the focus of future work.

Evolution in the relation between host galaxy virial mass and B -band absolute magnitude is more difficult to

interpret because M_B can both increase, due to recent episodes of star-formation and mergers, and decrease, due to fading in the stellar population. Although it was demonstrated earlier that our results as a function of M_B are consistent with the average host galaxy M_B fading by one magnitude from $z \sim 1$ and $z \sim 0$ while its dark matter halo does not evolve, our results as a function of stellar mass cast this simple interpretation into doubt. In particular, evolution in the M_{200}/M_* relation strongly suggests that the average halo mass of host galaxies is increasing from $z \sim 1$ to $z \sim 0$, since the stellar mass of host galaxies is most likely increasing with time (and, moreover, all currently favored cosmological models indicate that halos grow in mass with time). If halo mass increases significantly, host galaxies at $z \sim 1$ must fade by less than one magnitude (i.e. fading by less than L^* between these epochs) in order to reach the $z \sim 0$ M_{200}/L_B relation (cf. Figure 6, left panels).

8. SUMMARY

We summarize our main results and conclusions:

1. The $U - B$ color distribution of satellite host galaxies is indistinguishable from the colors of all galaxies (of similar luminosities), at both $z \sim 1$ and $z \sim 0$. Satellites of host galaxies at $z \sim 1$ are on average slightly *fainter* in the B -band relative to their host galaxy compared to $z \sim 0$, and host galaxies on average have a comparable number of satellites at both epochs.
2. The line-of-sight velocity dispersion, σ , of satellites increases with the average host galaxy luminosity, L_B , and stellar mass, M_* . In particular, $\sigma \propto M_*^{0.4 \pm 0.1}$ at both $z \sim 1$ and $z \sim 0$, while $\sigma \propto L_B^{0.6 \pm 0.1}$ at $z \sim 1$ and $\sigma \propto L_B^{0.4 \pm 0.1}$ at $z \sim 0$ (though it should be noted that these exponents are sensitive to the precise range of L_B and M_* over which the relation is fit). In addition, at fixed M_B red host galaxies have larger satellite velocity dispersions compared to blue hosts, both at $z \sim 1$ and $z \sim 0$.
3. The virial-to-stellar mass ratio, M_{200}/M_* , for host galaxies with $M_* \lesssim 10^{11} h^{-2} M_\odot$ increases by a factor of 1.1 ± 0.7 from $z \sim 1$ to $z \sim 0$; the ratio does not evolve significantly between these epochs. Host galaxies with stellar mass above $M_* \sim 10^{11} h^{-2} M_\odot$, which are predominantly red in restframe $U - B$ color, experience an increase in M_{200}/M_* of a factor of 4 ± 3 between these epochs.
4. The Millennium Run semi-analytic model of galaxy evolution reproduces the observed trends of M_{200}/M_* as a function of M_* at $z \sim 1$ quite well, while at $z \sim 0$ the model reproduces the shape of the $M_{200}/M_* - M_*$ but with a somewhat lower normalization compared to observations.

C.C. and F.P. acknowledge the “Palace Camp”, where none of this work took place. C.C. thanks Andrey Kravtsov, Simon White and Chris Wolf for useful discussions and Katherine Malinowska for a detailed reading of

the manuscript. The DEIMOS spectrograph was funded by NSF grant ARI92-14621 and by generous grants from the California Association for Research in Astronomy, and from UCO/Lick Observatory. The DEEP2 survey was founded under the auspices of the NSF Center for Particle Astrophysics. The bulk of this work was supported by National Science Foundation grants AST 95-29098 and 00-71198 to UCSC and AST 00-71048 to UCB. Additional support came from NASA grants AR-05801.01, AR-06402.01, and AR-07532.01 from the Space Telescope Science Institute, which is operated by AURA, Inc., under NASA contract NAS 5-26555. C.C. and F.P. acknowledge support from the Spanish MEC under grant PNAYA 2005-07789. A.L.C. and J.A.N. are supported by NASA through Hubble Fellowship grants HF-01182.01-A and HST-HF-01165.01-A, awarded by the Space Telescope Science Institute, which is operated by the Association of Universities for Research in Astronomy, Inc., for NASA, under contract NAS 5-26555. Some of the data presented herein were obtained at the W.M. Keck Observatory, which is operated as a scientific partnership among the California Institute of Technology, the University of California and the National Aeronautics and Space Administration. The Observatory was made possible by the generous financial support of the W.M. Keck Foundation. We also wish to recognize and acknowledge

the highly significant cultural role and reverence that the summit of Mauna Kea has always had within the indigenous Hawaiian community; it is a privilege to be given the opportunity to conduct observations from this mountain.

Funding for the Sloan Digital Sky Survey (SDSS) has been provided by the Alfred P. Sloan Foundation, the Participating Institutions, the National Aeronautics and Space Administration, the National Science Foundation, the U.S. Department of Energy, the Japanese Monbukagakusho, and the Max Planck Society. The SDSS Web site is <http://www.sdss.org/>.

The SDSS is managed by the Astrophysical Research Consortium (ARC) for the Participating Institutions. The Participating Institutions are The University of Chicago, Fermilab, the Institute for Advanced Study, the Japan Participation Group, The Johns Hopkins University, Los Alamos National Laboratory, the Max-Planck-Institute for Astronomy (MPIA), the Max-Planck-Institute for Astrophysics (MPA), New Mexico State University, University of Pittsburgh, Princeton University, the United States Naval Observatory, and the University of Washington.

This work made extensive use of the NASA Astrophysics Data System and of the `astro-ph` preprint archive at [arXiv.org](http://arxiv.org).

REFERENCES

- Abazajian, K. et al. 2004, *AJ*, 128, 502
 Adelman-McCarthy, J. K. et al. 2006, *ApJS*, 162, 38
 Baldry, I. K., Glazebrook, K., Brinkmann, J., Ivezić, Ž., Lupton, R. H., Nichol, R. C., & Szalay, A. S. 2004, *ApJ*, 600, 681
 Bell, E. F., McIntosh, D. H., Katz, N., & Weinberg, M. D. 2003, *ApJS*, 149, 289
 Bell, E. F. et al. 2004, *ApJ*, 608, 752
 Blanton, M. R. & Roweis, S. 2006, *ArXiv Astrophysics e-prints*
 Blanton, M. R. et al. 2003a, *AJ*, 125, 2276
 —. 2003b, *AJ*, 125, 2348
 —. 2005, *AJ*, 129, 2562
 Boehm, A. & Ziegler, B. L. 2006, *ArXiv Astrophysics e-prints*
 Borch, A., Meisenheimer, K., Bell, E. F., Rix, H.-W., Wolf, C., Dye, S., Kleinheinrich, M., Kovacs, Z., & Wisotzki, L. 2006, *A&A*, 453, 869
 Brainerd, T. G. 2005, *ApJ*, submitted, [arXiv:astro-ph/0409381](http://arxiv.org/abs/astro-ph/0409381)
 Brainerd, T. G., Blandford, R. D., & Smail, I. 1996, *ApJ*, 466, 623
 Brainerd, T. G. & Specian, M. A. 2003, *ApJ*, 593, L7
 Bullock, J. S. et al. 2001, *MNRAS*, 321, 559
 Bundy, K., Ellis, R. S., & Conselice, C. J. 2005a, *ApJ*, 625, 621
 Bundy, K. et al. 2005b, *ArXiv Astrophysics e-prints*
 Cattaneo, A., Dekel, A., Devriendt, J., Guiderdoni, B., & Blaizot, J. 2006, *ArXiv Astrophysics e-prints*
 Chen, J. et al. 2005, *ArXiv Astrophysics e-prints*
 Coil, A. L. et al. 2004, *ApJ*, 617, 765
 Cole, S., Lacey, C. G., Baugh, C. M., & Frenk, C. S. 2000, *MNRAS*, 319, 168
 Conroy, C., Wechsler, R. H., & Kravtsov, A. V. 2005a, *ArXiv Astrophysics e-prints*
 Conroy, C. et al. 2005b, *ApJ*, 635, 982
 Conselice, C. J., Bundy, K., Ellis, R. S., Brichmann, J., Vogt, N. P., & Phillips, A. C. 2005, *ApJ*, 628, 160
 Cooper, M. C., Newman, J. A., Madgwick, D. S., Gerke, B. F., Yan, R., & Davis, M. 2005, *ApJ*, 634, 833
 Croton, D. J. et al. 2006, *MNRAS*, 365, 11
 Davis, M., Gerke, B. F., & Newman, J. A. 2005, in *ASP Conf. Ser.* 339: *Observing Dark Energy*, ed. S. C. Wolff & T. R. Lauer, 128
 Davis, M. et al. 2003, in *Discoveries and Research Prospects from 6- to 10-Meter-Class Telescopes II*. Edited by Guhathakurta, Puragra. *Proceedings of the SPIE*, Volume 4834, pp. 161-172 (2003), ed. P. Guhathakurta, 161-172
 Dekel, A. & Birnboim, Y. 2006, *MNRAS*, 368, 2
 Diemand, J., Moore, B., & Stadel, J. 2004, *MNRAS*, 352, 535
 Erickson, L. K., Gottesman, S. T., & Hunter, J. H. 1987, *Nature*, 325, 779
 —. 1999, *ApJ*, 515, 153
 Faber, S. M. et al. 2003, in *Instrument Design and Performance for Optical/Infrared Ground-based Telescopes*. Edited by Iye, Masanori; Moorwood, Alan F. M. *Proceedings of the SPIE*, Volume 4841, pp. 1657-1669 (2003), ed. M. Iye & A. F. M. Moorwood, 1657-1669
 Faber, S. M. et al. 2005, *ApJ*, submitted, [arXiv:astro-ph/0506044](http://arxiv.org/abs/astro-ph/0506044)
 —. 2006, *ApJ*, in preparation
 Faltenbacher, A. & Diemand, J. 2006, *MNRAS*, 369, 1698
 Gerke, B. F. et al. 2005, *ApJ*, 625, 6
 —. 2006, *ApJ*, in preparation
 Ghigna, S., Moore, B., Governato, F., Lake, G., Quinn, T., & Stadel, J. 2000, *ApJ*, 544, 616
 Gnedin, O. et al. 2006, *ApJ*, in preparation
 Guzik, J. & Seljak, U. 2002, *MNRAS*, 335, 311
 Heymans, C. et al. 2006, *ArXiv Astrophysics e-prints*
 Hoekstra, H., Hsieh, B. C., Yee, H. K. C., Lin, H., & Gladders, M. D. 2005, *ApJ*, 635, 73
 Hoekstra, H., Yee, H. K. C., & Gladders, M. D. 2004, *ApJ*, 606, 67
 Hopkins, P. F., Hernquist, L., Cox, T. J., Di Matteo, T., Robertson, B., & Springel, V. 2006, *ApJS*, 163, 1
 Jones, L. R., Ponman, T. J., Horton, A., Babul, A., Ebeling, H., & Burke, D. J. 2003, *MNRAS*, 343, 627
 Kassin, S. et al. 2006a, *ApJ*, in preparation
 Kassin, S. A., de Jong, R. S., & Weiner, B. J. 2006b, *ApJ*, 643, 804
 Kauffmann, G. et al. 2003, *MNRAS*, 341, 33
 Kleinheinrich, M. et al. 2005, *ApJ*, submitted, [arXiv:astro-ph/0412615](http://arxiv.org/abs/astro-ph/0412615)
 Klypin, A. et al. 2006, *ApJ*, in preparation
 Little, B. & Tremaine, S. 1987, *ApJ*, 320, 493
 Mamon, G. A. & Lokas, E. L. 2005, *MNRAS*, 363, 705
 Mandelbaum, R., Seljak, U., Kauffmann, G., Hirata, C. M., & Brinkmann, J. 2006, *MNRAS*, 368, 715
 McGaugh, S. S. 2005, *ApJ*, 632, 859
 McKay, T. A. et al. 2002, *ApJ*, 571, L85
 Navarro, J. F., Frenk, C. S., & White, S. D. M. 1997, *ApJ*, 490, 493
 Navarro, J. F. et al. 2004, *MNRAS*, 349, 1039
 Noeske, K. et al. 2006, *ApJ*, in preparation
 Oke, J. B. & Gunn, J. E. 1983, *ApJ*, 266, 713
 Portinari, L. & Sommer-Larsen, J. 2006, *ArXiv Astrophysics e-prints*

- Prada, F. et al. 2003, ApJ, 598, 260
 Read, J. I. & Trentham, N. 2005, Royal Society of London Philosophical Transactions Series A, 363, 2693
 Spergel, D. N. et al. 2006, ArXiv Astrophysics e-prints
 Springel, V. et al. 2005, Nature, 435, 629
 Strauss, M. A. et al. 2002, AJ, 124, 1810
 Tasitsiomi, A., Kravtsov, A. V., Wechsler, R. H., & Primack, J. R. 2004, ApJ, 614, 533
 Vale, A. & Ostriker, J. P. 2004, MNRAS, 353, 189
 van den Bosch, F. C. 2002, MNRAS, 332, 456
 van den Bosch, F. C., Norberg, P., Mo, H. J., & Yang, X. 2004, MNRAS, 352, 1302
 Verheijen, M. A. W. 2001, ApJ, 563, 694
 Voit, G. M. 2005, Reviews of Modern Physics, 77, 207
 Wechsler, R. H., Bullock, J. S., Primack, J. R., Kravtsov, A. V., & Dekel, A. 2002, ApJ, 568, 52
 Weinmann, S. M., van den Bosch, F. C., Yang, X., & Mo, H. J. 2006, MNRAS, 366, 2
 Willmer, C. N. A. et al. 2006, ArXiv Astrophysics e-prints
 Wilson, G., Kaiser, N., Luppino, G. A., & Cowie, L. L. 2001, ApJ, 555, 572
 Yan, R., Madgwick, D. S., & White, M. 2003, ApJ, 598, 848
 Yan, R., White, M., & Coil, A. L. 2004, ApJ, 607, 739
 York, D. G. et al. 2000, AJ, 120, 1579
 Zaritsky, D., Smith, R., Frenk, C., & White, S. D. M. 1993, ApJ, 405, 464
 —. 1997, ApJ, 478, 39
 Zaritsky, D. & White, S. D. M. 1994, ApJ, 435, 599

APPENDIX

A. IMPACT OF SURVEY COMPLETENESS ON THE DERIVED AVERAGE HOST GALAXY HALO MASS

As described in §3.2, the DEEP2 survey obtains redshifts for $\sim 50\%$ of all galaxies with $R < 24.1$. In an incomplete galaxy catalog, we may identify a galaxy as isolated when in reality it has a bright companion that simply failed to be targeted. We assess the impact of incompleteness on the recovered velocity dispersion and halo mass by randomly diluting the SDSS survey and then searching for host galaxies and satellites. We show in Figure A9 the change in the measured halo mass, M_{200} , as a function of M_B and M_* , comparing host and satellite galaxies identified in the complete SDSS to the diluted SDSS. The recovered masses agree within $\sim 1\sigma$, which is encouraging, as this demonstrates that the modest incompleteness of the DEEP2 survey does not greatly change the recovered dispersion.

There is, however, a noticeable bias in the recovered masses: the diluted samples yield higher masses at a given host galaxy M_B and M_* . This is due to the inclusion of systems that are not truly isolated, but in fact reside in denser environments, which will have on average larger masses than isolated systems. We find that $\sim 35\%$ of host galaxies identified in the diluted sample are in fact not truly isolated. This number is comparable to the contamination rate found in Conroy et al. (2005b), who analyzed mock catalogs that included the same selection effects as the DEEP2 survey. This contamination fraction depends mildly on host luminosity, with sub-samples of brighter hosts having a lower contamination fraction than sub-samples of fainter hosts. This trend reflects the fact that brighter galaxies tend to be found in denser environments, so they are more likely to still have bright companions after dilution. The numerous bright companions will help prevent a bright galaxy from being falsely identified as isolated in the diluted sample, while the relative paucity of similar luminosity companions around fainter galaxies will make the identification of such a galaxy as (falsely) isolated in a diluted sample easier.

The average ratio between diluted and complete SDSS host galaxy halo masses is indicated by the dashed lines in Figure A9. We use these average mass corrections to arrive at host galaxy halo masses for 100% complete surveys, both at $z \sim 0$ and $z \sim 1$, when comparing against other work.

These falsely isolated host galaxies probably do not strongly effect the recovered velocity dispersion because the satellites that they contribute to the dV distribution resemble the interloper population: they are a small fraction of the total sample and they are more uniformly distributed in dV compared to satellites from truly isolated host galaxies.

Finally, we point out that any potential bias that may result from incompleteness will only impact the *absolute* σ and M_{200}/L values quoted herein. Results concerning the *relative* change in these quantities between $z \sim 1$ and $z \sim 0$ are likely not affected by incompleteness, since we have diluted the SDSS down to the same completeness as DEEP2 for those studies.

B. IMPACT OF CHANGING MEASUREMENT PARAMETERS

In this section we explore the effects of varying the parameters we have used when measuring velocity dispersions and deriving virial masses. Specifically, we explore the impact of changing the host-satellite search criteria or the number and size of the radial bins in which we measure velocity dispersions, and in addition we show that the derived masses are insensitive to the assumed halo concentration and velocity anisotropy. For simplicity, in the following tests we have selected one sample at $z \sim 0$ and one at $z \sim 1$ to illustrate our results (see Table B5), and the $z \sim 0$ sample has been diluted to match the completeness of the sample at $z \sim 1$, as mentioned previously. Our fiducial set of assumptions and parameters are an isotropic velocity distribution ($\beta = 0$), an NFW concentration of $c = 10$, a bin in projected separation between satellite and host of $R_p = [20, 150] h^{-1}$ kpc, and search criteria *A*.

We begin by testing assumptions that affect the measurement of velocity dispersions (and through this, the derived masses). In Table B5 we show the change in the derived virial mass when we use different search criteria and different radial bins. The primary effect of changing search criteria is that the number of satellites changes, which in turn alters the errors on the recovered velocity dispersion and virial mass. For example, using search criteria *B* or *C* at $z \sim 1$ results in only 30 and 32 satellites within $R_p = [20, 150] h^{-1}$ kpc, respectively, for the luminosity bins we consider in Table B5; hence the velocity dispersions and masses estimated for these samples are rather unstable. As can be gleaned

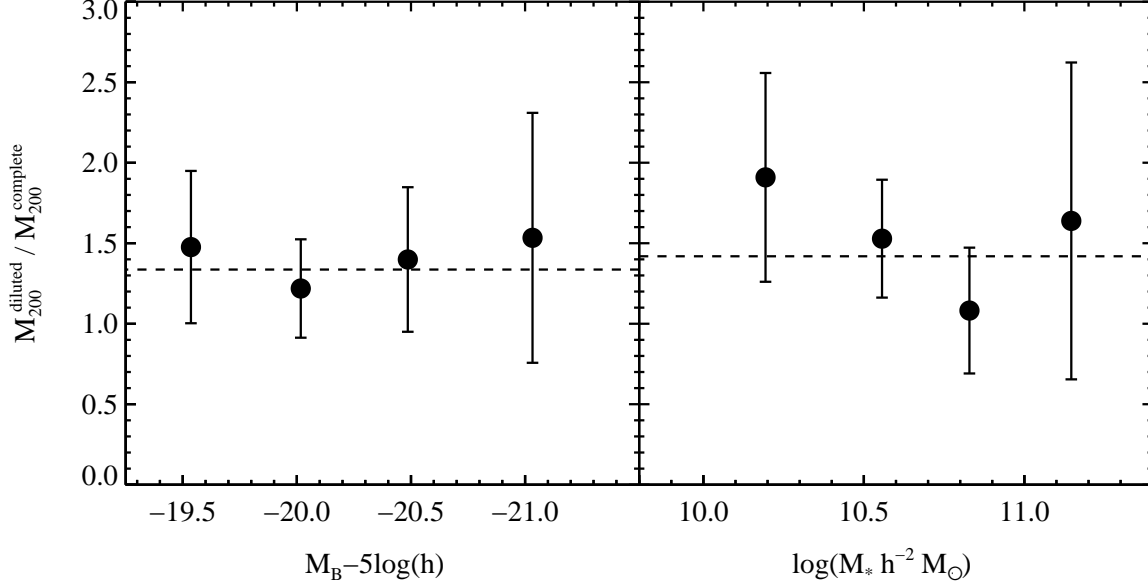


FIG. A9.— Ratio of host galaxy halo masses derived from the complete SDSS survey to masses derived from the SDSS survey diluted by 40% to match the completeness of the DEEP2 survey. The diluted sample yields systematically higher virial masses as a function of both M_B (left panel) and M_* (right panel). The dashed line in each panel represents the average $M_{200}^{\text{diluted}}/M_{200}^{\text{complete}}$ value. See Appendix A for details.

TABLE B5
DEPENDENCE OF DERIVED VIRIAL MASS ON VARIOUS PARAMETERS

Sample	Anisotropy		Concentration			Search Criteria			Radial bins (h^{-1} kpc)		
	$\beta = 0$	β_1	$c = 5$	$c = 10$	$c = 15$	A	B	C	[20, 100]	[20, 150]	[20, 200]
SDSS	2.8 ± 0.6	2.8 ± 0.6	2.8 ± 0.7	2.8 ± 0.6	2.8 ± 0.6	2.8 ± 0.6	3.0 ± 0.8	3.0 ± 1.0	2.3 ± 0.6	2.8 ± 0.6	3.5 ± 0.7
DEEP2	1.5 ± 0.6	1.6 ± 0.7	1.3 ± 0.6	1.5 ± 0.6	1.6 ± 0.6	1.5 ± 0.6	1.3 ± 1.0	2.5 ± 2.5	1.0 ± 0.5	1.5 ± 0.6	2.5 ± 1.0

NOTE. — The SDSS and DEEP2 samples include host galaxies with $-20.25 < M_B - 5 \log(h) < -19.75$ and $-21.0 < M_B - 5 \log(h) < -19.5$, respectively. All values are virial masses (M_{200}) in units of $10^{12} h^{-1} M_\odot$. The fiducial set of assumptions and parameters are $\beta = 0$, $c = 10$, search criteria A , and radial bin [20, 150] h^{-1} kpc. Each table entry is the result of varying only one of these parameters at a time. See Table 1 for details regarding the search criteria.

from the table, changing the search criteria or varying the radial binning results in changes in the recovered masses within 1σ of our fiducial estimates. Note also that using search criteria B at $z \sim 1$ and C at $z \sim 0$ amounts to using consistent isolation criteria in *comoving* coordinates (because in this case the projected separation scales as $(1+z)^{-1}$), and hence we conclude that using such coordinates, as opposed to physical coordinates, results in no significant change in our results.

We now test the impact on σ of using relatively bright satellites, i.e satellites that are only one magnitude fainter than their host galaxy. One might expect more massive (brighter) satellites to be out of virial equilibrium with the host galaxy since dynamical friction acts more efficiently on these satellites compared to less massive satellites. Using the complete SDSS sample, we measure the satellite velocity dispersion for hosts identified using search criteria A as a function of dM , the separation in brightness between the satellite and host galaxies. Specifically, we only include satellites that are at least 1.0, 1.5, 2.0, 2.5, and 3.0 magnitudes fainter than their host galaxy, and find that the dispersions estimated from these restricted samples all agree well within 1σ .

Since using different radial bins causes the largest changes in these tests, we have explored its effects in more detail. We have reconstructed the $\sigma - L$ and $\sigma - M_*$ relations using each set of radial bins and find no qualitative change in our results. In particular the exponents of these relations when using $R_p = [20, 200] h^{-1}$ kpc are the same at both $z \sim 1$ and $z \sim 0$, in agreement with the results shown in Figure 6. The results for the $R_p = [20, 100] h^{-1}$ kpc are noisier, as there are $\sim 50\%$ fewer satellites in this sample, but are also consistent with our fiducial results.

We now test assumptions that only affect the conversion between velocity dispersion and mass. In Table B5 we show

the effects of varying the concentration, c , or velocity anisotropy, β , on the recovered virial mass. We use concentrations of 5, 10, and 15, which span the range of typical concentrations for $\sim 10^{12} h^{-1} M_{\odot}$ dark matter halos for $0 < z < 1$. We test two forms of the velocity anisotropy, the isotropic case ($\beta = 0$), and a form suggested by Mamon & Lokas (2005) that is a good fit to a compilation of anisotropies derived from clusters within N -body simulations:

$$\beta_1(r) = \frac{1}{2} \frac{r}{r + r_a}, \quad (\text{B1})$$

where $r_a = 0.18 r_{200}$. This functional form has not been tested in galaxy-sized halos, though see the discussion in Appendix C.

At first glance it seems somewhat remarkable that the derived virial mass is almost independent of the concentration and velocity anisotropy parameters over the range tested. As it turns out, the line-of-sight velocity dispersion profile in the regime $50 < R_p < 150 h^{-1}$ kpc, which encompasses most of the satellites we use, is almost completely insensitive to concentration and anisotropy, while on both smaller and larger scales their effects are quite noticeable. We are, by necessity if not luck, probing a “sweet spot” in the velocity dispersion profile.

In addition, we have tested the sensitivity of the derived virial mass to the number of radial bins used to measure velocity dispersions. We can only perform this test for the SDSS sample due to the limited size of the DEEP2 sample. We have measured the velocity dispersion in three bins of projected separation, $R_p = [20 - 100], [100 - 200]$, and $[200 - 300] h^{-1}$ kpc, for the SDSS sample used in Table B5. We find a best fit virial mass of $M_{200} = 3.8 \pm 0.5 \times 10^{12} h^{-1} M_{\odot}$, which is within 1σ of the values quoted in Table B5 using only one radial bin. Furthermore, rebinning the *undiluted* SDSS sample results in a mass of $M_{200} = 2.6 \pm 0.6 \times 10^{12} h^{-1} M_{\odot}$. While we see a decline in the velocity dispersion profile for the undiluted sample in agreement with Prada et al. (2003), we see no decline for the diluted sample. This is likely due to the fact that the 35% of host galaxies in the diluted sample that are not truly isolated introduce noise into the dispersion measurement on large scales.

Finally, we turn to our assumption of an NFW (Navarro et al. 1997) characterization of the density profile. Recently, Prada et al. (2003) have detected a decline in the satellite velocity dispersion profile with increasing distance from the host galaxy at $z \sim 0$. This decline distinctly favors an NFW density profile over an isothermal distribution. However, we cannot distinguish between these and other density distributions at $z \sim 1$ because there are an insufficient number of satellites, making it difficult to bin more finely in radius and probe the velocity dispersion *profile*.

We are motivated to choose the same parameterization of the density profile at $z \sim 1$ and $z \sim 0$ because it seems unphysical for the density profile to drastically change, e.g. from isothermal to NFW, over this interval. Furthermore, an NFW-like density profile (notwithstanding minor deviations) appears to be a generic feature of hierarchical clustering, and is not sensitive to initial conditions or cosmological parameters (see e.g. Navarro et al. 1997, 2004). Note that our conclusions regarding the dependence of the satellite velocity dispersion on host luminosity and redshift are completely independent of density profile considerations.

C. ASSESSMENT OF ASSUMPTIONS

We identify three main assumptions inherent in using satellite galaxies to probe the virial dark matter mass of their hosts: 1) there is little scatter between host galaxy luminosity and dark matter halo virial mass, 2) satellites are fair tracers of the underlying dark matter velocity field, and 3) the velocity difference distribution of satellites and interlopers can be modeled as a Gaussian and a constant, respectively. These assumptions are well motivated both observationally and theoretically.

The first assumption (low scatter between mass and luminosity) must hold for our stacking procedure to work; it is motivated by the Tully-Fisher relation for disk-dominated galaxies and the Faber-Jackson relation for bulge-dominated galaxies. These relations have only a modest amount of scatter; typically 0.2 – 0.9 magnitudes at fixed velocity. The scatter is even smaller when these relations are quoted as a function of stellar mass or total baryonic mass (Verheijen 2001; McGaugh 2005). These tight correlations, with the assumption that the velocity measured probes the underlying halo mass, suggest that the scatter between halo mass and galaxy luminosity is not large, and hence that our stacking procedure is valid. In addition, models with a tight relation between galaxy luminosity and halo mass successfully reproduce a wide variety of observations (see e.g. Cole et al. 2000; Tasitsiomi et al. 2004; Conroy et al. 2005a; Croton et al. 2006; Vale & Ostriker 2004).

Under the assumption that satellite galaxies can be identified with subhalos in dissipationless N -body simulations, these simulations support our second assumption, that satellites are fair tracers of the underlying mass distribution. A number of studies have looked for a “velocity bias” between dark matter and subhalos. Recent work has suggested that such a bias, defined as the ratio between the velocity dispersion of subhalos and dark matter, is about 10% when averaged over entire clusters (Ghigna et al. 2000; Diemand et al. 2004). In fact, when Faltenbacher & Diemand (2006) identify subhalos in a simulated cluster in such a way that their spatial distribution matches observed galaxies, they find no velocity bias. Although no study has systematically investigated the velocity bias in galaxy-size halos, Prada et al. (2003) showed that subhalos identified in a simulated galaxy-sized halo accurately reflect the underlying mass distribution. Admittedly, the velocity bias of the most massive subhalos, which should correspond to the satellites studied here (since we use relatively bright satellites, which are likely associated with the most massive subhalos), has not been adequately investigated. Nevertheless, we conclude that satellite galaxies, should be fair tracers of the underlying dark matter halo mass to $\sim 10\%$ or better.

The second and third assumptions have been tested in conjunction by a number of authors. Prada et al. (2003) identified satellite galaxies with subhalos in dissipationless N -body simulations, and artificially added in interloper

galaxies uniformly in phase space. They found that for an isolated Milky-Way sized dark matter halo, the Gaussian plus constant parameterization accurately recovers the velocity dispersion profile of subhalos, which in turn accurately reflects the underlying dark matter halo mass.

van den Bosch et al. (2004) also tested these assumptions using cosmological mock galaxy catalogs at $z \sim 0$, and found that the simple Gaussian plus constant parameterization accurately recovers the velocity dispersion of host galaxies as a function of galaxy luminosity. These authors additionally investigated the impact of orbital anisotropy and a spatial (anti-) bias of the satellite galaxies, and found the resulting effects on the recovered dispersion to be minimal. Specifically, when using satellites within one-third of the virial radius from the host galaxy, they found that if β changes from -0.5 to 0.5 then the velocity dispersion changes by $< 10\%$.

These assumptions have also been tested at $z \sim 1$ by Conroy et al. (2005b) who used cosmological simulations into which mock galaxies were inserted using a halo model approach (see Yan et al. 2003, 2004, for details concerning these mock catalogs). These authors found that the velocity dispersion profile of mock galaxies accurately reflects the underlying halo mass, and that interlopers can be effectively modeled as a constant component to the velocity difference distribution.

Consistency between weak-lensing and satellite measurements of M_{200}/L in past studies gives further confirmation that satellites are fair tracers of the underlying dark matter velocity field (unless both satellite dynamics and weak lensing measurements are biased in a similar way). McKay et al. (2002) compared the dependence of the mass-to-light ratio on luminosity derived from both satellite dynamics and weak lensing measurements, and found agreement within 1σ . Furthermore, both weak lensing studies (Guzik & Seljak 2002; Hoekstra et al. 2004, 2005; Kleinheinrich et al. 2005; Mandelbaum et al. 2006) and satellite dynamics (McKay et al. 2002; Prada et al. 2003; Brainerd & Specian 2003; van den Bosch et al. 2004) have found that the derived virial mass scales with host luminosity as $M \propto L^\alpha$ with $1.0 \lesssim \alpha \lesssim 1.5$. The range in α can be at least partially explained by the different regimes (isolated galaxies vs. groups and clusters) and photometric bands probed.